Mouse gingival single-cell transcriptomic atlas: An activated fibroblast subpopulation guides oral barrier immunity in periodontitis

Takeru Kondo [1,2], Annie Gleason [1,3], Hiroko Okawa [1,2], Akishige Hokugo [1,4], Ichiro Nishimura [1]*

[1]Weintraub Center for Reconstructive Biotechnology, UCLA School of Dentistry, Los Angeles, CA 90095, USA

[2]Division of Molecular and Regenerative Prosthodontics, Tohoku University Graduate School of Dentistry, Sendai, Miyagi 980-8575, Japan

[3]UCLA Bruin in Genomics Summer Program,

[4]Regenerative Bioengineering and Repair Laboratory, Division of Plastic and Reconstructive Surgery, Department of Surgery, David Geffen School of Medicine at UCLA, Los Angeles, CA 90095, USA

*Corresponding Author:

Ichiro Nishimura, DDS, DMSc, DMD

Weintraub Center for Reconstructive Biotechnology

UCLA School of Dentistry

Box 951668, CHS B3-087, Los Angeles, CA 90095, USA

Tel: +1 (310) 794-7612, Fax: +1 (310) 825-6345

E-mail: inishimura@dentistry. ucla.edu

Abstract

Periodontitis, one of the most common non-communicable diseases, is characterized by chronic oral inflammation and uncontrolled tooth supporting alveolar bone resorption. Its underlying mechanism to initiate aberrant oral barrier immunity has yet to be delineated. Here, we report a unique fibroblast subpopulation activated to guide oral inflammation (AG fibroblasts) identified in a single-cell RNA sequencing gingival cell atlas constructed from the mouse periodontitis models. AG fibroblasts localized beneath the gingival epithelium and in the cervical periodontal ligament responded to the ligature placement and to the discrete application of Toll-like receptor stimulants to mouse maxillary tissue. The upregulated chemokines and ligands of AG fibroblasts linked to the putative receptors of neutrophils in the early stages of periodontitis. In the established chronic inflammation, neutrophils together with AG fibroblasts appeared to induce type 3 innate lymphoid cells (ILC3s) that were the primary source of interleukin-17 cytokines. The comparative analysis of *Rag2*-/- and *Rag2γc*-/- mice suggested that ILC3 contributed to the cervical alveolar bone resorption interfacing the gingival inflammation. We propose that AG fibroblasts function as a previously unrecognized surveillant to initiate gingival inflammation leading to periodontitis through the AG fibroblast-neutrophil-ILC3 axis.

Introduction

The oral mucosa is one of the most active barrier tissues in the human body [1, 2] and oral barrier immunity acts as a crucial surveillance system, which must defend from pathogenic organisms, while ensuring sustained tolerance of commensal microbes and harmless antigens [3]. However, once this gingival inflammation progresses, adjacent alveolar bone supporting the cervical area of the dentition is subjected to a localized, but often severe, osteoclastic bone resorption, resulting in tooth loss and disruption of the maxillofacial structure [4]. Periodontitis is not only the most frequent cause of tooth loss in adults [5], but also, globally, ranks among the most significant contributors to poor health and decreased quality of life, imposing substantial economic and healthcare burdens [6]. It is therefore acutely important to elucidate the molecular mechanisms underlying the initiation of gingival inflammation, in order to facilitate the development of effective preventive and therapeutic measures for this debilitating condition.

The postulated pathological framework has been reconstructed from animal models [7, 8], harvested immune cell analyses, and oral microbial associations [4, 9, 10]. For example, the ligature-induced periodontitis mouse model has shown that fully developed periodontal inflammation is closely associated with the abundant recruitment and excessive activation of neutrophils [11] and pathological induction of interleukin (IL)-17–secreting proinflammatory effector $CD4^+$ T helper (Th)17 cells [12]. Based on our current understanding of osteoimmunology, it was hypothesized that these pathological immune cells activate osteoclasts, leading to induction of periodontal alveolar bone resorption [13, 14]. However, the precise cascade of events leading to this disease outcome has not been fully deciphered.

Investigation of the molecular mechanisms underlying interaction between different inflammatory cell fractions in immunological disorders is an intense area of research. Prior studies have shown that chemokines are involved in the trafficking and activation of inflammatory cells

during both homeostasis and disease-associated inflammation [14]. These small proteins, which typically contain disulfide cysteine–cysteine (CC) and cysteine–X–cysteine (CXC) molecular signatures, act as ligands for cellular receptors that modulate inflammatory signaling pathways [15]. Such chemokine–receptor networks direct the migration of inflammatory cells, potentially amplifying the resulting tissue damage. However, increasing evidence suggests that in addition to immune cells, barrier tissue stromal cells are involved in innate immune cell regulation [16-19]. We and others have found that oral fibroblasts secrete cytokines and chemokines in response to microbial stimuli or a proinflammatory environment, suggesting a possible mechanism by which they may regulate immune cell function [8, 20]. Therefore, a comprehensive elucidation of chemokine–receptor signaling networks will likely need to include all types of gingival cells.

In the present study, to better understand the pathways contributing to chronic oral inflammation, we constructed the gingival single-cell transcriptomic atlas of the ligature-induced periodontitis mouse model as well as the newly developed mouse model of maxillary topical application (MTA) of pathological oral microbial biofilm component(s), discretely mimicking the initial events of gingival inflammation and degradation. Here we report a novel subpopulation of fibroblasts activated to guide chronic inflammation (AG fibroblasts). Our findings suggest that chemokines and ligands derived from AG fibroblasts bind to and activate receptors involved in neutrophil and lymphocytes. We further show that in the fully developed chronic gingival inflammation of the ligature-induced periodontitis model, *Cd4*$^{-}$ innate lymphoid cells (ILCs) predominantly produce proinflammatory IL-17 cytokines and provide evidence that type 3 ILCs (ILC3s) are responsible for cervical alveolar bone resorption in mice—a pathological feature consistent with the human periodontitis disease phenotype. Thus, the results from this study identify the AG fibroblast–neutrophil–ILC3 axis as a previously unrecognized mechanism contributing to pathological inflammation in periodontitis.

Results

Alterations in major cell type proportions during periodontitis development

The alveolar bone and gingival tissue surrounding the maxillary second molar of C57BL/6J mice presented healthy connective tissue supporting the dentition with minimal CD45+ immune cell infiltration and well-developed collagen architecture (**Figure 1A – figure supplement 1A**). The placement of a ligature around the maxillary left second molar[21] induced a localized and small gingival connective tissue degradation and infiltration of CD45+ immune cells near the cervical area (**Figure 1B**). The noticeable gingival defect and more prominent though still localized CD45+ immune cell infiltration developed after Day 3 following ligature placement (**Figure 1C – figure supplement 1A, 1B**). On Day 7, the gingival connective tissue was largely degraded, and chronic inflammation was developed (**Figure 1D – figure supplement 1A, 1B**). Three-dimensional (3D) reconstruction of micro-computed tomography (microCT) images (**figure supplement 1C**) further revealed a reduction in alveolar bone height starting from Day 3, which progressively increased on Day 7 (**figure supplement 1D, 1E**). Overall, the observed pattern of periodontal tissue degradation was consistent with that reported in previous studies [22, 23].

Left-side palatal gingiva tissue was harvested from mice on Day 0 (*i.e.*, healthy gingiva without ligature placement) and on Days 1, 4, and 7 after ligature placement, and gingival cells were dissociated for single-cell RNA sequencing (scRNA-seq) [8, 24]. On Days 0 and 1, the major cell types identified included epithelial cells expressing cadherin 1 (*Cdh1*) [25] and type XVII collagen (*Col17a1*) [26], fibroblasts expressing type I collagen (*Col1a1*) [27] and lumican (*Lum*) [28], B cells expressing membrane spanning 4 domains A1 (*Ms4a1*) [29] and cluster of differentiation 79A (*Cd79a*) [30], T cells expressing epsilon subunit of T cell receptor complex (*Cd3e*) [31] and cluster of differentiation 5 (*Cd5*) [32], and myeloid cells expressing lysozyme 2 (*Lyz2)* [33] and integrin subunit alpha M (*Itgam*) [34] (**Figure 1E and F—figure supplement 2**).

110 On Days 4 and 7, an additional endothelial cell fraction expressing selectin P (*Selp*) [35] and
111 selectin E (*Sele*) [36] emerged (**Figure 1E and F—figure supplement 2**), suggesting increased
112 inflammatory neovascularization with the progression of periodontal inflammation. The proportion
113 of B cells was increased on Day 1, and the proportion of myeloid cells increased progressively
114 from Day 4 to 7 (**Figure 1F**). In addition, the proportion of fibroblasts was increased on Day 7
115 (**Figure 1F**).
116

117 **Fibroblasts activated to guide leukocyte migration in periodontitis development**

118 We previously identified two distinct subpopulations of gingival fibroblasts, differentiated by
119 expression of type XIV collagen (*Col14a1*) [8], and these were also detected in our current scRNA-
120 seq data from Day 0 to 7 (**Figure 2A**). Gene ontogeny (GO) enrichment analysis of the *Col14a1*-
121 expressing fibroblast subpopulation revealed expression of major gene clusters related to immune
122 regulation, including "Regulation of leukocyte migration" (**Figure 2B**). This immune regulatory
123 phenotype appears to be unique to *Col14a1*-expressing fibroblasts, which are therefore referred
124 to as 'fibroblasts activated to guide leukocyte migration' or AG fibroblasts. The other
125 subpopulation of *Col1a1*-expressing fibroblasts appeared to keep typical fibroblastic features and
126 is thus referred to as KT fibroblasts (**Figure 2C**). GO analysis suggested that KT fibroblasts
127 primarily maintained connective tissue remodeling but did not express an immune regulatory
128 phenotype. An additional fibroblast subpopulation expressing smooth muscle aortic actin 2
129 (*Acta2*) was detected on Day 7, and these were identified as myofibroblasts [37] (MF) (**Figure
130 2A**). We found that the proportions of KT and AG fibroblasts were equal on Day 0 and on Days 1
131 and 4 after ligature placement (**Figure 2E, 2F**). However, on Day 7, the proportion of AG
132 fibroblasts decreased, and the MF fraction emerged (**Figure 2E, 2F**).
133

134 **AG fibroblasts and immune surveillance in early periodontitis development**

135 To further characterize AG fibroblasts and their "Regulation of leukocyte migration" phenotype,
136 we analyzed expression of CC motif chemokine ligands (CCLs) and CXC motif chemokine ligands
137 (CXCLs) within fibroblast subpopulations in our scRNA-seq dataset [13]. Results show that AG
138 fibroblasts activated expression of *Ccl8, Ccl11, Ccl19, Cxcl1, Cxcl10*, and *Cxcl12* immediately
139 after ligature placement on Days 1 and 4 (**Figure 3A**). Chemokine expression levels then
140 decreased on Day 7, suggesting that AG fibroblasts might initiate early leukocyte migration into
141 gingival tissue. Given that activation of Toll-like receptors (TLR) is known to increase chemokine
142 expression, we further assessed expression of TLRs in fibroblast subpopulations. We found that
143 AG fibroblasts displayed temporal activation of *Tlr2, Tlr3*, and *Tlr4* expression on Days 1 and 4
144 (**Figure 3B**). Similarly, the TLR downstream genes *Myd88, Irak1, Map3k7*, and *RelA* were also
145 expressed on Days 1 and 4 (**Figure 3B**). These data suggest that AG fibroblasts may guide the
146 establishment of an early inflammatory environment within the gingiva and thereby promote
147 periodontitis pathogenesis.

148 To validate the presence of AG fibroblasts, Day 1 gingiva and periodontal tissue histological
149 sections were subjected to immunohistochemistry with antibodies against COL14A1 and CXCL12
150 (**Figure 3C**). We detected COL14A1- and CXCL12-positive AG fibroblasts localized near gingival
151 epithelial cells in the connective tissue papillae and free gingiva, as well as in the cervical zone of
152 the periodontal ligament (PDL) space (**Figure 3C**). We note that this localization pattern of AG
153 fibroblasts appears to be highly suitable for early immune surveillance during periodontitis
154 pathogenesis. Thus, we have hypothesized that AG fibroblasts initially sense the pathological
155 stress including oral microbial stimuli through TLRs and secrete inflammatory signals through
156 chemokine expression.

157

158 **AG fibroblasts induced by maxillary topical application (MTA) of unmethylated cytidine**
159 **phosphate guanosine oligonucleotide (CpG ODN) and of *Porphyromonas gingivalis***
160 **lipopolysaccharide (LPS)**

161 To further characterize the behavior of AG fibroblasts, we used the recently developed
162 maxillary topical application (MTA) model without the placement of a ligature. The MTA model
163 applied oral microbial biofilm directly to the maxillary gingiva and held under a custom-made oral
164 appliance (**Figure 4A**) for 1 hr. Four days after the topical application, mouse maxillary tissue was
165 harvested for histological analysis and for scRNA-seq (**Figure 4B**) [8]. We previously reported
166 that oral microbial biofilm and its extracellular polymeric substances such as extracellular DNA,
167 but not planktonic microbes, induced initial periodontal tissue reaction in the MTA model [8]. The
168 present study discretely applied ligands of TLR9 and TLR2/4: unmethylated CpG ODN and *P.*
169 *gingivalis* LPS, respectively; using the MTA model. CpG ODN induced the expression of
170 cathepsin K (Ctsk) in the periodontal ligament (PDL) and gingival connective tissue (**Figure 4C**)
171 validating the previous report [8]. Furthermore, there were signs of localized Ctsk+ osteoclastic
172 activities on the surface of alveolar bone (**Figure 4C**).

173 The scRNA-seq gingival cell composition of the MTA of CpG ODN and LPS indicated the
174 early periodontitis pattern (**Figure 4E**) consistent with Day 1 scRNA-seq of the ligature-induced
175 periodontitis (**Figure 1F**). The MTA of CpG ODN and LPS identified AG fibroblasts along with KT
176 fibroblasts, whereas the MTA of LPS induced the additional MF (**Figure 4E**). The further analysis
177 demonstrated the expression of CCL and CXCL chemokines by AG fibroblasts activated by the
178 MTA of CpG ODN and LPS (**Figure 4F**). CpG ODN and LPS are sensed by Toll-Like Receptor 9
179 (TLR9) and TLR2/4, respectively. The scRNA-seq of MTA of CpG ODN did not capture the
180 transcriptional activation of *Tlr9*, while the downstream effector genes such as *Myd99*, *Irak1* and
181 *RelA* were found upregulated in AG fibroblasts (**Figure 4G**). The MTA of LPS appeared to

182 upregulate *Tlr2* and *Tlr4* gene transcription of AG fibroblasts and of MF albeit at lesser degrees
183 (**Figure 4G**). These results indicated that AG fibroblasts were activated by CpG ODN and LPS
184 through the MTA model, while these microbial elements appeared to exert different reactions.
185

186 **Myeloid cell composition and activity during periodontitis development**

187 The infiltration of proinflammatory neutrophils into the gingiva has been extensively characterized
188 in this mouse model of periodontitis [11, 38]. Here, we found that macrophages expressing cluster
189 of differentiation 86 (*Cd86*) [39] and integrin subunit alpha X (*Itgax)* [40] were predominant on
190 Day 0 in the myeloid cell fraction from healthy gingiva (**Figure 5A, 5B—figure supplement 3**). In
191 contrast, the proportion of neutrophils expressing CXC motif chemokine receptor (*Cxcr2*) [41] and
192 G0/G1 switch gene 2 (*G0s2*) [42] increased after ligature placement and during periodontitis
193 development from Day 1 to 7 (**Figure 5A, 5B—figure supplement 3**), suggesting continuous
194 neutrophil infiltration into the early and established gingival lesion. Moreover, after ligature
195 placement, gingival neutrophils upregulated the expression of triggering receptor expressed on
196 myeloid cells 1 (*Trem1*), indicating that these cells are activated and participating in the
197 amplification of inflammatory signals [43, 44] (**Figure 5C**). Strikingly, the *Trem1*-expressing
198 activated neutrophils also show upregulation of matrix metalloproteinase 9 (*Mmp9*; **Figure 5C**)—
199 a protein associated with extracellular matrix degeneration within gingival tissue [45]. We further
200 detected expression of tumor necrosis factor (*Tnf*) and transforming growth factor beta 1 (*Tgfb1*)
201 in both macrophages and neutrophils on Day 0 and after ligature placement (**Figure 5D**).
202 Collectively, these myeloid cell behaviors are consistent with those reported in prior studies on
203 periodontitis development, thus validating our scRNA-seq data.

204 Myeloid cells are also known to stimulate other immune cells through the expression of CCL
205 and CXCL chemokines, many of which are associated with periodontitis development [46]. Our

206 scRNA-seq analysis revealed that macrophages expressed *Ccl2*, *Ccl9*, Cxcl4, and *Cxcl6*, and
207 neutrophils expressed *Ccl3*, *Ccl4*, *Ccl6*, *Cxcl2,* and *Cxcl3* throughout periodontitis development
208 (**Figure 5E, 5F**). These data suggest that chemokines and cytokines produced by macrophages
209 and neutrophils in inflamed tissue may amplify and polarize the immune response toward chronic
210 gingival inflammation.
211

212 **Role of AG fibroblasts in myeloid cell activation**

213 The interaction between chemokine ligands and their receptors has been extensively studied.
214 Here, to evaluate the interaction between chemokine ligands strongly expressed by AG fibroblasts
215 and chemokine receptors in innate immune cells, we matched AG fibroblast-expressed
216 chemokines to expression of their putative receptors in myeloid cells. Results show that AG
217 fibroblasts may regulate macrophages via the expression *Ccl8* and *Ccl11*, which encode
218 chemokines that can interact with CC chemokine receptors (CCRs) encoded by *Ccr2* and *Ccr5* in
219 macrophages. Similarly, gene expression signatures suggest that AG fibroblast-mediated
220 neutrophil regulation may occur through CCL8–CCR1, CXCL1–CXCR2, and CXCL12–CXCR4
221 interactions (**Figure 6A**). Notably, all chemokine–receptor pairs are expressed throughout
222 periodontitis development, although expression of factors mediating the interaction between AG
223 fibroblasts and macrophages was decreased on Day 7.

224 Intercellular communication may occur via other ligand–receptor interactions, which
225 induce downstream target gene expression in recipient cells. Here, we performed NicheNet
226 analysis to identify potential interactions between gingival fibroblasts and myeloid cells, revealing
227 a trend toward increasing ligand–target interactions between fibroblasts and myeloid cells from
228 Day 1 to Day 7 (**Figure 6B**). On Day 1, ligand expression was present primarily in AG fibroblasts,
229 whereas on Day 7, MFs also exhibited prominent ligand expression (**Figure 6C**). Analysis of target

230 gene expression revealed that both macrophages and neutrophils expressed receptors capable
231 of interacting with AG fibroblast ligands on Day 1. In contrast, on Day 7, receptor expression was
232 almost exclusively present in neutrophils, suggesting these cells are primarily targeted by MFs
233 and AG fibroblasts at later stages of periodontitis development (**Figure 6D**).

234 The chemokine-receptor interaction was also suggested between AG fibroblasts and
235 myeloid cells in the MTA of CpG DON (**Figure 6E**). However, in the MTA of LPS, macrophage
236 lacked the detectable expression of chemokine receptor and the AG fibroblastic chemokine
237 interaction appeared to be limited to neutrophils (**Figure 6E**).

238

239 **Expression of osteoclastogenic cytokines**

240 Macrophage-colony stimulating factor (M-CSF), encoded by *Csf1,* and receptor activator of
241 nuclear factor kappa-B ligand (RANKL), encoded by *Tnfsf11,* are known to play critical roles in
242 osteoclast induction [47]. We found that in the ligature-induced periodontitis model, the expression
243 of M-CSF was detected in various cell types including fibroblasts (**Figure 7A),** whereas the
244 RNAKL expression was more restricted to fibroblasts and T cells (**Figure 7B**). AG fibroblasts
245 consistently expressed M-CSF from Day 0 to Day 7 and neutrophils started to express M-CSF in
246 Day 4 and Day 7 (**Figure 7C**). The expression of RNAKL was detected in AG fibroblasts but not
247 in myeloid cells (**Figure 7D**). T cells and type 3 innate lymphoid cells (ILC3; see below) were also
248 shown to express M-CSF and RNAKL (**Figure 7C, 7D**).

249 The MTA of CpG ODN and LPS suggested the AG fibroblasts were one of the predominant
250 cellular sources of M-CSF (**Figure 7E**). By contrast, the expression of RNAKL was only detected
251 in AG fibroblasts of the MTA of CpG ODN and LPS did not seem to induce RANKL expression in
252 the MTA model (**Figure 7F**). The osteoclastic activity found in the MTA of CpG ODN (**Figure 4D**)
253 might be induced by M-CSF and RANKL derived from AG fibroblasts.

254

255 **Helper T (Th) cells, cytotoxic T (Tc) cells, regulatory T (Treg) cells and innate lymphoid**
256 **cells (ILCs) in periodontitis development**

257 Our scRNA-seq dataset found that the Day 0 healthy gingiva exclusively contained Th cells
258 expressing *Cd4* [48]. However, after ligature placement, Tc cells expressing *Cd8* [48] emerged,
259 and on Day 7, *Cd4*$^{-}$*Zbtb16*$^{+}$ ILCs and *Cd4*$^{+}$*Foxp3*$^{+}$ Treg cells [49] were also detected (**Figure 8A,**
260 **8B**). The ILCs expressed *Nfil3*, a basic leucine zipper (bZIP) transcription factor required for ILC
261 development [50] (**Figure 8C**). However, to our surprise, expression of *Rorc*, *Il17a*, and *Il17f* was
262 detected in ILCs (**Figure 8C**), indicating that this gingival subpopulation is predominantly
263 composed of type 3 ILCs (ILC3s). ILC3s and Th17 cells share similar regulatory functions.
264 However, the role of ILC3s in the development of periodontitis has not been fully deciphered.

265

266 **ILC3s are critical for cervical alveolar bone resorption in the mouse periodontitis model**

267 We thus examined the role of ILC3s in periodontitis pathogenesis by measuring ligature-induced
268 gingival defects and alveolar bone resorption in *Rag2*$^{-/-}$ mice, which lack functional B, Th, and Tc
269 cells, and *Rag2*–IL-2 receptor common gamma (*Il2rg*) double-knockout mice (*Rag2γc*$^{-/-}$), lacking
270 all lymphocytes including ILCs. After ligature placement, we found that alveolar bone loss was
271 decreased in *Rag2*$^{-/-}$ mice and nearly eliminated in *Rag2γc*$^{-/-}$ mice (**Figure 8D**). MicroCT image
272 analysis indicated a better perseveration of alveolar bone structure in *Rag2γc*$^{-/-}$ mice, relative to
273 the other groups (**Figure 8E—figure supplement 4A, 4B**). However, gingival defects developed
274 similarly in wild-type (WT), *Rag2*$^{-/-}$, and *Rag2γc*$^{-/-}$ mice (**figure supplement 4C, 4D**).

275 Histologically, osteoclastic resorption lacunae were observed on the alveolar bone surface
276 at the cervical PDL and tooth apex PDL zones in WT mice (**Figure 8F, 8G**). In addition, we
277 detected a significant decrease in the number of tartrate-resistant acid phosphatase (TRAP)-

278 positive osteoclasts in the cervical PDL zone of *Rag2γc*$^{-/-}$ mice (**Figure 8H**) and in the apical PDL
279 zone of both *Rag2*$^{-/-}$ and *Rag2γc*$^{-/-}$ mice (**Figure 8I**). Collectively, these data suggest that ILC3s,
280 not Th17 cells, are responsible for cervical alveolar bone resorption in the mouse periodontitis
281 model, a pathological phenotype consistent with human disease (**figure supplement 4E, 4F**).
282

283 **The role of AG fibroblasts and neutrophils in ILC3 development in periodontitis**

284 Based on our present data, we hypothesize that ILC3s within the gingival tissue play a
285 pathological role in cervical alveolar bone resorption in our mouse model. We therefore aimed to
286 identify the cells that promote ILC3 development in mice. Similar to Th17 cells, ILC3 development
287 was shown to be triggered by IL-6 and IL-23a [51, 52]. A survey of our scRNA-seq data identified
288 epithelial cells, fibroblasts, and myeloid cells as the source of *Il6* in gingival tissue (**Figure 9A**).
289 On Days 1 and 4 following ligature placement, AG fibroblasts primarily expressed *Il6,* whereas
290 neutrophils became the predominant source on Day 7. We further found that gingival epithelial
291 cells comprise at least four different subpopulations, plus an additional group displaying an
292 epithelial–mesenchymal transition (EMT) phenotype on Day 7; *Il6* was expressed by several of
293 these epithelial subpopulations, including the EMT subgroup (**Figure 9A—figure supplement**
294 **5A–D**). *Il23a* was also detected AG fibroblasts and myeloid cells (**Figure 9B**), with expression
295 present in all epithelial cell subsets at various points in periodontitis development (**Figure 9B—**
296 **figure supplement 5D**).

297 Lastly, we evaluated potential interactions between chemokine ligands expressed by AG
298 fibroblasts and neutrophils and chemokine receptors in innate immune cells. Our data suggest
299 the presence of a chemokine–receptor association between ILC3s and both AG fibroblasts
300 (**Figure 9C**) and neutrophils (**Figure 9D**), although interactions with other innate immune cells
301 are also possible. NicheNet analysis further identified potential ligand–target gene associations

302 between lymphocytes, including ILC3s, and both fibroblasts (**Figure 9E**) and myeloid cells
303 (**Figure 9F**). Ligand expression was more prominent in AG fibroblasts than in other fibroblast
304 subpopulations (**Figure 9G**) and elevated in neutrophils relative to macrophages (**Figure 9H**).
305 Additionally, target gene expression was detected in ILC3s, although it was not specific to these
306 cells (**Figure 9I, 9J**). Thus, in total, our data suggest a regulatory role for a newly identified AG
307 fibroblast subpopulation in the gingiva, which appears to orchestrate chronic gingival inflammation,
308 at least in the early stages, and to promote alveolar bone resorption via stimulation of neutrophils
309 and ILC3s.
310

311 **Discussion**

312 The present study revealed that the gene signature of a unique and previously uncharacterized
313 subpopulation of gingival fibroblasts, referred to as AG fibroblasts, could possess the functional
314 capability to serve as an oral immune surveillant and to orchestrate the initiate gingival
315 inflammation. Oral barrier immunity presents a complex interaction between different types of
316 immune cells to protect and maintain the oral environment and structure. Given the frequent
317 exposure to a diverse commensal and pathological microbiome, physical and chemical insults,
318 and dietary and airborne antigens, the oral barrier immune mechanism must resiliently establish
319 the highly tolerant homeostasis [53]. This oral immune homeostasis mechanism is not yet fully
320 understood to date; however, the aberrant oral immune response and gingival chronic
321 inflammation leading to periodontitis have provided an important clue to elucidate the oral barrier
322 immunity.

323 The previous studies suggested gingival intraepithelial γδT cells [54], a subset of
324 neutrophils [55], macrophages [56], and dendritic cells [57] should serve the candidate immune
325 surveillant in the oral barrier tissue. These immune cells recognize the pathological signals
326 through the TLR sensing mechanism. TLR2$^{-/-}$, TLR4$^{-/-}$, TLR2&4$^{-/-}$ [58] and TLR9$^{-/-}$ [59, 60] mice
327 exhibited the reduced alveolar bone loss in various mouse periodontitis models, suggesting that
328 TLRs indeed played an important role in developing discordant oral barrier immunity. However,
329 these studies did not identify the TLR-carrying surveillant cells centrally involved in initiating the
330 chronic gingival inflammation.

331 It has been suggested that TLR-expressing gingival fibroblasts may regulate innate
332 immune responses [61, 62]. In the present study, we found that not all gingival fibroblasts acquired
333 an immune-sensing capability, but rather, AG fibroblasts represented a distinct fibroblast
334 subpopulation, capable of responding to microbial and tissue damage signals to serve initiate

335 immune surveillance. To test if TLR ligands stimulate the AG fibroblast activation, we applied a
336 newly developed mouse system employing the discrete MTA model [8]. The present study used
337 TLR9 ligand: CpG ODN; and TLR2/4 ligand: LPS. Topical application of these TLR ligands to the
338 maxillary gingival tissue activated AG fibroblasts and increased expression of CC and CXC
339 chemokines (**Figure 4F**). It was noted that the CpG ODN application did not upregulate *Tlr9*
340 expression, while the LPS application increased *Tlr2/4* expression. *TLR9* mRNA level has not
341 been fully correlated to the chronic inflammatory diseases; however, the pathological activation
342 of TLR9 caused the discordant downstream inflammation [63]. In the present study, the differential
343 expression of the TLR downstream signaling molecules suggested the ligand specific response
344 by AG fibroblasts. In fact, both stimulants increased the expression of myeloid differentiation
345 marker 88 (*Myd88*), IL1R-associated kinase (*Irak*), mitogen-activated protein kinase (*Map3k7*)
346 and NF-kB subunit *RelA* (**Figure 4G**), suggesting that the corresponding TLRs were indeed
347 stimulated [64, 65]. The *Tlr* expression pattern of Day 1 AG fibroblasts was similar to that of the
348 MTA of CpG ODN, whereas the Day 4 AG fibroblasts resembled the *Tlr* expression pattern of the
349 MTA of LPS (**Figure 3B**). It is tempting to speculate that microbial DNA/TLR9 activation of AG
350 fibroblasts may initiate the early pathological process followed by the LPS/TRL2/4 stimulation in
351 the more established periodontal inflammation. Taken together, we hypothesize that AG
352 fibroblasts sensitively detect the microbial signals and play a previously unrecognized role in
353 innate immune regulation during the early periodontitis development.

354 One of the major observations in the present study was that AG fibroblasts clearly
355 upregulated the chemokine expression only after the pathological stimulation. CCL and CXCL
356 chemokines orchestrate the chronic inflammation through the ligation and activation of their
357 putative chemokine receptors in a specific mechanism. For example, neutrophils express a
358 relatively limited number of chemokine receptors—CXCR2, CXCR4, and CCR1 [66, 67].

359 Therefore, neutrophil migration and trafficking to the affected gingiva as well as its pathological
360 transformation in chronic periodontitis patients [11, 68, 69] may be guided through the specific
361 chemokine-receptor interaction. Consistent with prior studies, we detected the expression of
362 these chemokine receptors in gingival neutrophils, and they were linked to the chemokine ligands
363 expressed by AG fibroblasts—CXCL1, CXCL12, and CCL8, respectively (**Figure 6).** In addition,
364 neutrophils can respond to various chemo-attractants that modulate and finetune various cellular
365 behaviors, such as migration direction, adhesion strength, and functional heterogeneity [70]. Here ,
366 we observed evidence for substantial intracellular communication between AG fibroblasts and
367 neutrophils through ligand–target gene interactions (**Figure 6**). Although validation of each
368 putative ligand–receptor interaction is beyond the scope of this study, our data suggest that AG
369 fibroblasts support neutrophil trafficking in both early and established periodontitis lesions.

370 A primary pathological consequence of periodontitis is uncontrolled alveolar bone resorption,
371 leading to tooth loss, which is thought to be mediated by osteoimmune pathways involving IL-17–
372 expressing Th17 cells [71]. Surprisingly, analysis of our scRNA-seq revealed that the expression
373 of *Rorc, Il17a*, and *Il17f* was not detected in $CD4^+$ Th cells, but rather, in lymphocytes with ILC
374 characteristics (**Figure 8**). ILCs share phenotypic and functional features with $CD4^+$ T cells,
375 although they lack antigen-specific T cell receptors [50]. The gingival ILCs expressed *Rorc*, *Il17a,*
376 and *Il17f,* but not *Tbx21* and *Gata3,* indicating that they were type 3 ILCs (ILC3s). Notably, recent
377 clinical studies have reported the presence of ILCs in gingiva from human periodontitis patients
378 [72, 73] and leptin receptor–deficient mice [74], although their pathological contributions have not
379 been fully elucidated.

380 In the present study, we further explored the role of ILC3s in periodontitis-associated bone
381 loss using *Rag2*$^{-/-}$ and *Rag2γc*$^{-/-}$ mice. *Rag2*$^{-/-}$ mutation prevents V(D)J recombination required for
382 generating immunoglobulin and T cell receptors, resulting in the production of functionally

383 immature B and T cells, including Th17 cells. However, ILCs do not undergo genomic receptor
384 rearrangements and, thus, are unaffected by *Rag2*$^{-/-}$ mutation. In contrast, *Rag2γc*$^{-/-}$ mice have
385 the additional *Il2rg*$^{-/-}$ mutation, which disables common γ chain cytokines (γc). Therefore, in
386 addition to non-functional B and T cells, these animals also have defective γc-dependent ILCs.
387 The ligature-placed *Rag2*$^{-/-}$ mice exhibited a reduced number of osteoclasts in the apical PDL area,
388 indicative of reduced bone resorption in this root apical region. By contrast, *Rag2γc*$^{-/-}$ mice
389 demonstrated a significant loss of bone resorption in both the cervical and apical PDL areas
390 (**Figure 8**). Human periodontitis induces the localized alveolar bone resorption at the cervical PDL
391 zone interfacing the gingival inflammatory legion. In contrast, apical alveolar bone resorption is
392 observed in clinical cases of root canal infection (apical periodontitis). Therefore, our findings
393 suggest that ILC3s, which are differentially impacted by *Rag2γc*$^{-/-}$ and *Rag2*$^{-/-}$ mutations, may be
394 primarily responsible for human periodontitis-like cervical alveolar bone resorption near the site
395 of gingival inflammation.

396 Differentiation of ILC3s and Th17 cells is mediated by similar environmental cues, with IL-6
397 and IL-23a playing critical roles in both pathways [75, 76]. Our present scRNA-seq data (**Figure**
398 **9**) suggest that AG fibroblasts and neutrophils are the primary cellular sources of *Il6* during the
399 early and later stages, respectively, of periodontitis development. In contrast, *Il23a* was found to
400 be expressed by a variety of cell types, such as AG fibroblasts, myeloid cells, and multiple subsets
401 of epithelial cells, including those with an EMT phenotype [77]. Further, CC and CXC chemokine–
402 receptor associations between ILC3s and both AG fibroblasts and neutrophils appeared to be
403 non-specific. Therefore, our data suggest that rather than a specific trigger, the collective gingival
404 environment, which includes AG fibroblasts, might contribute to ILC3 differentiation.

405 In conclusion, based on our present findings, we propose that a previously unrecognized
406 AG fibroblast subpopulation in the gingiva can facilitate immune surveillance and participate in

407 the pathological regulation of innate immune cells, such as proinflammatory neutrophils, within
408 oral barrier tissue (**Figure 10**). Moreover, we hypothesize that ILC3s in the inflamed gingiva play
409 a critical role in pathological alveolar bone resorption in the mouse model of periodontitis and,
410 potentially, in human disease. Thus, the newly proposed AG fibroblast–neutrophil–ILC3 axis may
411 hold valuable clues for unraveling the pathological mechanisms underlying periodontitis
412 development. Moreover, these findings also provide a basis for investigation of new preventive
413 and therapeutic strategies to contain oral barrier inflammation and potentially sever the link
414 between periodontitis and debilitating non-communicative metabolic and cardiovascular diseases.
415

416 **Methods**

417 **Animal care**

418 All protocols for animal experiments were reviewed and approved by the University of California
419 Los Angeles (UCLA) Animal Research Committee (ARC# 2003-009) and followed the Public
420 Health Service Policy for the Humane Care and Use of Laboratory Animals and the UCLA Animal
421 Care and Use Training Manual guidelines. C57BL/6J WT, *Rag2*$^{-/-}$, and *Rag2γc*$^{-/-}$ mice were
422 purchased from the Jackson Laboratory (Bar Harbor, ME, USA). Animals had free access to
423 regular rodent diet and water and were maintained in standard housing conditions with 12-h
424 light/dark cycles in the Division of Laboratory Animal Medicine at UCLA.

425

426 **Evaluation of gingival defect and alveolar bone resorption in a ligature-induced mouse**
427 **model of periodontitis**

428 A silk thread was gently tied around the left maxillary second molar of 8- to 12-week-old female
429 WT, *Rag2*$^{-/-}$, and *Rag2γc*$^{-/-}$ mice under general inhalation anesthesia with isoflurane (Henry Schein,
430 Melville, NY, USA). On Days 1, 3, and 7 after ligature placement, WT mice were randomly chosen
431 and euthanized by 100% CO_2 inhalation. WT mice without ligature placement were used as Day
432 0 pre-periodontitis control. *Rag2*$^{-/-}$ and *Rag2γc*$^{-/-}$ mice were euthanized on Day 7. The palatal
433 tissue was digitally photographed, and maxillae were harvested and fixed in 10% buffered
434 formalin (Thermo Fisher Scientific, Waltham, MA, USA). The gingival defect area was measured
435 from digital photographs, using the ImageJ Java-based image-processing program (NIH,
436 Bethesda, MD, USA), and normalized to the circumferential area of the maxillary first molar. Fixed
437 maxillae were subjected to microCT imaging at an energy level of 60 kV and 166 μA, and 3D
438 images were reconstructed from microCT scans (Skyscan 1275: Bruker, Billerica, MA, USA).
439 Alveolar bone loss was assessed at three sites (mesiobuccal cusp, distobuccal cusp, and distal

440 cusp) of the first molar, two sites (mesiobuccal cusp and distobuccal cusp) of the second molar,
441 and one site (buccal cusp) of the third molar by measuring the distance from the cementoenamel
442 junction (CEJ) to the alveolar bone crest (ABC) on the buccal and palatal side of the alveolar bone.
443 Total bone loss was calculated from the six-site total CEJ–ABC distance. The bone volume/total
444 volume (BV/TV) ratio, bone surface, trabecular number (Tb.N), and trabecular thickness (Tb.Th)
445 in the buccal side of alveolar bone of the second molar were determined using the proprietary
446 analysis program (CTan: Bruker, Billerica, MA, USA). Statistical analysis to assess differences
447 among multiple experimental groups was performed using one-way analysis of variance (ANOVA)
448 with Tukey's multiple-comparison test; $p < 0.05$ was considered to be statistically significant.
449

450 **Evaluation of gingival effect in the maxillary topical application (MTA) model**

451 We have developed a method to apply chemical therapeutic agents topically to the mouse
452 maxillary tissue [24, 78]. We used the maxillary topical application (MTA) model to apply oral
453 microbial components [8]. The present study used the MTA model using 1 μg/ml unmethylated
454 CpG oligonucleotide (CpG ODN: InvivoGen, San Diego, CA) or *P. gingivalis* lipopolysaccharide
455 (LPS: InvivoGen). First, a custom-made oral appliance was fabricated using clear dental resin,
456 covering the maxillary/palatal tissue between the molars. Mice were anesthetized and placed on
457 a supine position. CpG ODN (3 μl) or LPS (3 μl) was pipetted over the maxillary tissue and the
458 oral appliance was placed to hold the solution with a bite block for 1 hr in an anesthetization
459 chamber. Mice were then transferred to the operation table and the oral appliance and bite block
460 were removed. In general, there was no remaining solution in the mouth. Mice were returned to
461 the cage in the vivarium. On Day 4 of the MTA, mice were euthanized by 100% CO2 inhalation
462 and the maxillary tissue was harvested and fixed with 10% buffered formalin for histological
463 evaluation.

464

465 **Histological analysis**

466 Fixed maxillae were decalcified in 10% EDTA (Sigma–Aldrich) for 3 weeks and then embedded
467 in paraffin. Histological cross-sections were stained with hematoxylin and eosin (HE) and
468 evaluated on a light microscope. Adjacent paraffin sections (4 μm) were subjected to a heat-
469 induced epitope retrieval procedure and then immunohistochemically stained with polyclonal
470 antibodies to CD45 (#PA5-11671, Thermo Fisher Scientific), COL14A1 (#PA5-49916, Thermo
471 Fisher Scientific), CXCL12 (#PA5-30603, Thermo Fisher Scientific), or Ctsk (PA5-14270, Thermo
472 Fisher Scientific) at the suggested dilution, followed by secondary antibody application,
473 diaminobenzidine staining, and methylene blue counterstaining.

474 Using maxillary cross-sections of WT, Rag2$^{-/-}$, and Rag2$^{-/-}$γc$^{-/-}$ mice, osteoclasts were
475 evaluated by TRAP staining using a commercially available kit (Acid Phosphatase TRAP kit,
476 Sigma–Aldrich), according to the manufacturer's instructions. TRAP-positive cells were counted
477 in the 0.01-mm^2 area. Statistical analysis to assess the differences among multiple experimental
478 groups was performed using one-way ANOVA with Tukey's multiple-comparison test; $p < 0.05$
479 was considered to be statistically significant.

480

481 **Single cell dissociation from mouse maxillary gingiva**

482 On Days 1, 4, and 7 after ligature placement, and on Day 4 of the MTA of CpG ODN or LPS, mice
483 were euthanized by 100% CO_2 inhalation. And maxillary gingival tissues (n = 4 per group) were
484 harvested from freshly isolated mouse maxillae.

485 *Collagenase II treatment*: The tissues were cut into 1-mm pieces and placed immediately into
486 digestion buffer, containing 1-mg/ml collagenase II (Life Technologies, Thermo Fisher Scientific,
487 Waltham, MA, USA), 10-units/ml DNase I (Sigma–Aldrich, St. Louis, MO, USA), and 1% bovine

488 serum albumin (BSA; Sigma–Aldrich) in Dulbecco's Modified Eagle Medium (DMEM; Life
489 Technologies). The tissues were incubated in digestion buffer for 20 min at 37 °C on a shaker at
490 150 rpm and then passed through a 70-μm cell strainer. The collected cells were pelleted at 1,500
491 rpm for 10 min at 4 °C and resuspended in phosphate-buffered saline (PBS; Life Technologies),
492 supplemented with 0.04% BSA (Cell suspension A).

493 *Trypsin treatment*: Immediately following collagenase II treatment, tissues were incubated in
494 0.25% trypsin (Life Technologies) and 10-units/ml DNase I for 30 min at 37 °C on a 150-rpm
495 shaker. Trypsin was neutralized with fetal bovine serum (Life Technologies), and the tissues were
496 passed through a 70-μm cell strainer and washed with DMEM. The collected cells were then
497 pelleted at 1,500 rpm for 10 min at 4 °C and resuspended in PBS with 0.04% BSA (Cell
498 suspension B). Cell suspension A and Cell suspension B were combined in one tube. An equal
499 number of combined cell suspensions A and B from four animals per group were combined for
500 scRNA-seq analysis (10X Genomics, San Francisco, CA, USA).

501

502 **Cell clustering and Identification**

503 Cell Ranger was used to align reads, generate feature–barcode matrices, and perform clustering
504 and gene expression analyses on the scRNA-seq data, and the output from this program was
505 analyzed using the R-program Seurat (https://satijalab.org/seurat/). Cells with <2,400 genes
506 detected or >1% mitochondrial gene expression were filtered out as low-quality cells. Individual
507 gene counts for each cell were divided by the total gene counts for that cell and multiplied by a
508 scale factor of 10,000; natural-log transformation was then applied to the counts. The
509 FindVariableFeatures function was used to select 2,000 variable genes with default parameters,
510 and the ScaleData function was used to scale and center the counts in the dataset. Principal
511 component analysis and Uniform Manifold Approximation and Projection dimensional reduction

512 were performed on variably expressed genes. The cluster markers were found using the
513 FindAllMarkers function, and cell types were manually annotated based on the cluster markers.
514 Cell types were assigned based on expression of cell marker genes, and gene expression within
515 different cell types was displayed using dot plots and violin plots.
516

517 **Functional annotation and pathway enrichment analysis**

518 Annotation and visualization of GO terms were performed by Metascape
519 (http://metascape.org/gp/index.html#/main/step1). The top-100 differentially expressed genes in
520 each population were input and filtered with the term "immune". Filtered genes were then input,
521 and only "biological process" gene sets were retrieved from the GO database.
522

523 **Ligand–target matrix prediction**

524 NicheNet (v.1.0.0, https://github.com/saeyslab/nichenetr) was used to predict interactions
525 between cell types. In brief, the integrated Seurat object containing each cell subpopulation was
526 input into the NicheNet Seurat wrapper. Sender cells and receiver cells were determined, and
527 interactions between active ligands expressed by sender cells and target receptors expressed by
528 receiver cells were predicted based on information in signaling and ligand–receptor databases.
529

530 **Acknowledgements**

531 We thank Dr. Connie Lee of Division of Periodontology at UCLA School of Dentistry for her
532 guidance on the clinical manifestations of human periodontitis. We also thank Dr. Yunfeng Li of
533 the Translational Pathology Core Laboratory, Department of Pathology and Laboratory Medicine,
534 David Geffen School of Medicine at UCLA for her immunohistology work. This study was

supported by NIH grants R01DE022550, R44DE025524, and C06RR014529 and by SINTX Technologies.

Author contributions

I.N. conceptualized the project and obtained funding. T.K., H.O. and A.H. performed animal studies. H.O. collected micro-CT data from the animal model. T.K. and A.G. performed scRNA-seq and data analysis. T.K. and I.N. drafted the manuscript. All authors gave final approval and agreed to be accountable for all aspects of the work.

Competing interests

I.N. is a consultant for FUJI FILM Corp and BioVinc LLC and received a research fund from SINTX Technologies, Inc. I.N. and A.H. received a research fund from Maruho Co. Ltd. The other authors declare no competing interests.

Data availability statement

We specify where the data supporting the results of this study can be found and provide hyperlinks to publicly archived datasets analyzed or generated during the study, where applicable. scRNA-seq data are found in NIH Gene Expression Omnibus (GSE228635).

555 ## References

556 1. Abusleme, L., et al., *The subgingival microbiome in health and periodontitis and its*
557 *relationship with community biomass and inflammation.* ISME J, 2013. **7**(5): p. 1016-25.
558 2. Belkaid, Y. and O.J. Harrison, *Homeostatic Immunity and the Microbiota.* Immunity, 2017.
559 **46**(4): p. 562-576.
560 3. Moutsopoulos, N.M. and H.M. Moutsopoulos, *The oral mucosa: A barrier site participating in*
561 *tissue-specific and systemic immunity.* Oral Dis, 2018. **24**(1-2): p. 22-25.
562 4. Lamont, R.J., H. Koo, and G. Hajishengallis, *The oral microbiota: dynamic communities and*
563 *host interactions.* Nat Rev Microbiol, 2018. **16**(12): p. 745-759.
564 5. Helal, O., et al., *Predictors for tooth loss in periodontitis patients: Systematic review and meta-*
565 *analysis.* J Clin Periodontol, 2019. **46**(7): p. 699-712.
566 6. Peres, M.A., et al., *Oral diseases: a global public health challenge.* Lancet, 2019. **394**(10194):
567 p. 249-260.
568 7. Lin, P., et al., *Application of Ligature-Induced Periodontitis in Mice to Explore the Molecular*
569 *Mechanism of Periodontal Disease.* Int J Mol Sci, 2021. **22**(16): p. 8900.
570 8. Kondo, T., et al., *Oral microbial extracellular DNA initiates periodontitis through gingival*
571 *degradation by fibroblast-derived cathepsin K in mice.* Commun Biol, 2022. **5**(1): p. 962.
572 9. Hajishengallis, G. and T. Chavakis, *Local and systemic mechanisms linking periodontal*
573 *disease and inflammatory comorbidities.* Nat Rev Immunol, 2021. **21**(7): p. 426-440.
574 10. Shokeen, B., et al., *Effect of Calcium Ion Supplementation on Oral Microbial Composition and*
575 *Biofilm Formation In Vitro.* Microorganisms, 2022. **10**(9): p. 1780.
576 11. Hajishengallis, G., *New developments in neutrophil biology and periodontitis.* Periodontol
577 2000, 2020. **82**(1): p. 78-92.
578 12. Hasiakos, S., et al., *Calcium Signaling in T Cells and Chronic Inflammatory Disorders of the*
579 *Oral Cavity.* J Dent Res, 2021. **100**(7): p. 693-699.
580 13. Cekici, A., et al., *Inflammatory and immune pathways in the pathogenesis of periodontal*
581 *disease.* Periodontol 2000, 2014. **64**(1): p. 57-80.
582 14. Sokol, C.L. and A.D. Luster, *The chemokine system in innate immunity.* Cold Spring Harb
583 Perspect Biol, 2015. **7**(5): p. a016303.
584 15. Hughes, C.E. and R.J.B. Nibbs, *A guide to chemokines and their receptors.* FEBS J, 2018.
585 **285**(16): p. 2944-2971.
586 16. Hodzic, Z., et al., *IL-33 and the intestine: The good, the bad, and the inflammatory.* Cytokine,
587 2017. **100**: p. 1-10.

588 17. Ina, K., et al., *Intestinal fibroblast-derived IL-10 increases survival of mucosal T cells by*
589 *inhibiting growth factor deprivation- and Fas-mediated apoptosis.* J Immunol, 2005. **175**(3): p.
590 2000-9.
591 18. Pinchuk, I.V., et al., *PD-1 ligand expression by human colonic myofibroblasts/fibroblasts*
592 *regulates CD4+ T-cell activity.* Gastroenterology, 2008. **135**(4): p. 1228-1237, 1237 e1-2.
593 19. Cheng, H.W., et al., *CCL19-producing fibroblastic stromal cells restrain lung carcinoma growth*
594 *by promoting local antitumor T-cell responses.* J Allergy Clin Immunol, 2018. **142**(4): p. 1257-
595 1271 e4.
596 20. Williams, D.W., et al., *Human oral mucosa cell atlas reveals a stromal-neutrophil axis*
597 *regulating tissue immunity.* Cell, 2021. **184**(15): p. 4090-4104 e15.
598 21. Abe, T. and G. Hajishengallis, *Optimization of the ligature-induced periodontitis model in mice.*
599 J Immunol Methods, 2013. **394**(1-2): p. 49-54.
600 22. Tamura, H., et al., *Analysis of Experimental Ligature-Induced Periodontitis Model in Mice.*
601 Methods Mol Biol, 2021. **2210**: p. 237-250.
602 23. Marchesan, J., et al., *An experimental murine model to study periodontitis.* Nat Protoc, 2018.
603 **13**(10): p. 2247-2267.
604 24. Okawa, H., et al., *Mechanism of bisphosphonate-related osteonecrosis of the jaw (BRONJ)*
605 *revealed by targeted removal of legacy bisphosphonate from jawbone using competing inert*
606 *hydroxymethylene diphosphonate.* Elife, 2022. **11**: p. e76207.
607 25. Groeger, S. and J. Meyle, *Oral Mucosal Epithelial Cells.* Front Immunol, 2019. **10**: p. 208.
608 26. Kamaguchi, M., et al., *High Expression of Collagen XVII Compensates for its Depletion*
609 *Induced by Pemphigoid IgG in the Oral Mucosa.* J Invest Dermatol, 2018. **138**(8): p. 1707-1715.
610 27. Takahashi, A., et al., *Autocrine regulation of mesenchymal progenitor cell fates orchestrates*
611 *tooth eruption.* Proc Natl Acad Sci U S A, 2019. **116**(2): p. 575-580.
612 28. Lallier, T.E., A. Spencer, and M.M. Fowler, *Transcript profiling of periodontal fibroblasts and*
613 *osteoblasts.* J Periodontol, 2005. **76**(7): p. 1044-55.
614 29. Bruno, K.F., et al., *Characterization of inflammatory cell infiltrate in human dental pulpitis.*
615 Int Endod J, 2010. **43**(11): p. 1013-21.
616 30. Sparger, E.E., et al., *Investigation of immune cell markers in feline oral squamous cell*
617 *carcinoma.* Vet Immunol Immunopathol, 2018. **202**: p. 52-62.
618 31. Alcover, A., B. Alarcon, and V. Di Bartolo, *Cell Biology of T Cell Receptor Expression and*
619 *Regulation.* Annu Rev Immunol, 2018. **36**: p. 103-125.
620 32. Fujihashi, K., et al., *Immunoregulatory function of CD3+, CD4-, and CD8- T cells. Gamma*
621 *delta T cell receptor-positive T cells from nude mice abrogate oral tolerance.* J Immunol, 1989.
622 **143**(11): p. 3415-22.

623 33. Cross, M., et al., *Mouse lysozyme M gene: isolation, characterization, and expression studies.*
624 Proc Natl Acad Sci U S A, 1988. **85**(17): p. 6232-6.
625 34. Okubo, M., et al., *M2-polarized macrophages contribute to neovasculogenesis, leading to*
626 *relapse of oral cancer following radiation.* Sci Rep, 2016. **6**: p. 27548.
627 35. Gotsch, U., et al., *Expression of P-selectin on endothelial cells is upregulated by LPS and TNF-*
628 *alpha in vivo.* Cell Adhes Commun, 1994. **2**(1): p. 7-14.
629 36. Komatsu, T., et al., *E-selectin mediates Porphyromonas gingivalis adherence to human*
630 *endothelial cells.* Infect Immun, 2012. **80**(7): p. 2570-6.
631 37. Sasaki, H., et al., *Neuronal PAS Domain 2 (Npas2)-Deficient Fibroblasts Accelerate Skin*
632 *Wound Healing and Dermal Collagen Reconstruction.* Anat Rec (Hoboken), 2020. **303**(6): p.
633 1630-1641.
634 38. Silva, L.M., L. Brenchley, and N.M. Moutsopoulos, *Primary immunodeficiencies reveal the*
635 *essential role of tissue neutrophils in periodontitis.* Immunol Rev, 2019. **287**(1): p. 226-235.
636 39. Lam, R.S., et al., *Macrophage depletion abates Porphyromonas gingivalis-induced alveolar*
637 *bone resorption in mice.* J Immunol, 2014. **193**(5): p. 2349-62.
638 40. Agarbati, S., et al., *Prognostic Relevance of Macrophage Phenotypes in High-grade Oral*
639 *Tongue Squamous Cell Carcinomas.* Appl Immunohistochem Mol Morphol, 2021. **29**(5): p. 359-
640 365.
641 41. Hashim, A., et al., *Loss of Neutrophil Homing to the Periodontal Tissues Modulates the*
642 *Composition and Disease Potential of the Oral Microbiota.* Infect Immun, 2021. **89**(12): p.
643 e0030921.
644 42. Zhang, F., et al., *Activation of G0S2 is coordinated by recruitment of PML/RARalpha and*
645 *C/EBPepsilon to its promoter during ATRA-induced APL differentiation.* J Leukoc Biol, 2017.
646 **101**(3): p. 655-664.
647 43. Bouchon, A., J. Dietrich, and M. Colonna, *Cutting edge: inflammatory responses can be*
648 *triggered by TREM-1, a novel receptor expressed on neutrophils and monocytes.* J Immunol,
649 2000. **164**(10): p. 4991-5.
650 44. Dopheide, J.F., et al., *Critical limb ischaemia is characterised by an increased production of*
651 *whole blood reactive oxygen species and expression of TREM-1 on neutrophils.* Atherosclerosis,
652 2013. **229**(2): p. 396-403.
653 45. Corotti, M.V., et al., *Immunolocalization of matrix metalloproteinases-2 and -9 during apical*
654 *periodontitis development.* Arch Oral Biol, 2009. **54**(8): p. 764-71.
655 46. Souto, G.R., et al., *Relationship between chemokines and dendritic cells in human chronic*
656 *periodontitis.* J Periodontol, 2014. **85**(10): p. 1416-23.
657 47. Teitelbaum, S.L., *Bone resorption by osteoclasts.* Science, 2000. **289**(5484): p. 1504-8.

658 48. Mahanonda, R., et al., *Memory T cell subsets in healthy gingiva and periodontitis tissues.* J
659 Periodontol, 2018. **89**(9): p. 1121-1130.
660 49. Wei, L., M. Xu, and H. Xiong, *An update of knowledge on the regulatory role of Treg cells in*
661 *apical periodontitis.* Oral Dis, 2021. **27**(6): p. 1356-1365.
662 50. Eberl, G., et al., *Innate lymphoid cells. Innate lymphoid cells: a new paradigm in immunology.*
663 Science, 2015. **348**(6237): p. aaa6566.
664 51. Bielecki, P., et al., *Skin-resident innate lymphoid cells converge on a pathogenic effector state.*
665 Nature, 2021. **592**(7852): p. 128-132.
666 52. Powell, N., et al., *Interleukin 6 Increases Production of Cytokines by Colonic Innate Lymphoid*
667 *Cells in Mice and Patients With Chronic Intestinal Inflammation.* Gastroenterology, 2015.
668 **149**(2): p. 456-67 e15.
669 53. Moutsopoulos, N.M. and J.E. Konkel, *Tissue-Specific Immunity at the Oral Mucosal Barrier.*
670 Trends Immunol, 2018. **39**(4): p. 276-287.
671 54. Chen, Y., et al., *gammadeltaT cells in oral tissue immune surveillance and pathology.* Front
672 Immunol, 2022. **13**: p. 1050030.
673 55. Fine, N., et al., *Distinct Oral Neutrophil Subsets Define Health and Periodontal Disease States.*
674 J Dent Res, 2016. **95**(8): p. 931-8.
675 56. Metcalfe, S., et al., *Innate Phagocyte Polarization in the Oral Cavity.* Front Immunol, 2021.
676 **12**: p. 768479.
677 57. Hovav, A.H., *Dendritic cells of the oral mucosa.* Mucosal Immunol, 2014. **7**(1): p. 27-37.
678 58. Lin, M., et al., *Different engagement of TLR2 and TLR4 in Porphyromonas gingivalis vs.*
679 *ligature-induced periodontal bone loss.* Braz Oral Res, 2017. **31**: p. e63.
680 59. Kim, P.D., et al., *Toll-Like Receptor 9-Mediated Inflammation Triggers Alveolar Bone Loss in*
681 *Experimental Murine Periodontitis.* Infect Immun, 2015. **83**(7): p. 2992-3002.
682 60. Crump, K.E., et al., *Interplay of Toll-Like Receptor 9, Myeloid Cells, and Deubiquitinase A20*
683 *in Periodontal Inflammation.* Infect Immun, 2017. **85**(1): p. e00814-16.
684 61. Qian, S.J., et al., *Single-Cell RNA Sequencing Identifies New Inflammation-Promoting Cell*
685 *Subsets in Asian Patients With Chronic Periodontitis.* Front Immunol, 2021. **12**: p. 711337.
686 62. Naruishi, K., *Biological Roles of Fibroblasts in Periodontal Diseases.* Cells, 2022. **11**(21): p.
687 3345.
688 63. Dragasevic, S., et al., *Importance of TLR9-IL23-IL17 axis in inflammatory bowel disease*
689 *development: Gene expression profiling study.* Clin Immunol, 2018. **197**: p. 86-95.
690 64. Takeshita, F., et al., *Cutting edge: Role of Toll-like receptor 9 in CpG DNA-induced activation*
691 *of human cells.* J Immunol, 2001. **167**(7): p. 3555-8.
692 65. Takeda, K. and S. Akira, *TLR signaling pathways.* Semin Immunol, 2004. **16**(1): p. 3-9.

693 66. Sabroe, I., et al., *Regulation of human neutrophil chemokine receptor expression and function*
694 *by activation of Toll-like receptors 2 and 4.* Immunology, 2005. **115**(1): p. 90-8.
695 67. Huston, J., 3rd and J.R. Muhm, *Solitary pulmonary nodules: evaluation with a CT reference*
696 *phantom.* Radiology, 1989. **170**(3 Pt 1): p. 653-6.
697 68. Kolaczkowska, E. and P. Kubes, *Neutrophil recruitment and function in health and*
698 *inflammation.* Nat Rev Immunol, 2013. **13**(3): p. 159-75.
699 69. Tecchio, C. and M.A. Cassatella, *Neutrophil-derived chemokines on the road to immunity.*
700 Semin Immunol, 2016. **28**(2): p. 119-28.
701 70. Metzemaekers, M., M. Gouwy, and P. Proost, *Neutrophil chemoattractant receptors in health*
702 *and disease: double-edged swords.* Cell Mol Immunol, 2020. **17**(5): p. 433-450.
703 71. Deng, J., et al., *The Th17/Treg cell balance: crosstalk among the immune system, bone and*
704 *microbes in periodontitis.* J Periodontal Res, 2022. **57**(2): p. 246-255.
705 72. Brown, J.L., et al., *Enrichment of Innate Lymphoid Cell Populations in Gingival Tissue.* J Dent
706 Res, 2018. **97**(12): p. 1399-1405.
707 73. Dutzan, N., et al., *Characterization of the human immune cell network at the gingival barrier.*
708 Mucosal Immunol, 2016. **9**(5): p. 1163-1172.
709 74. Wang, Q., et al., *Single-Cell Transcriptomic Atlas of Gingival Mucosa in Type 2 Diabetes.* J
710 Dent Res, 2022. **101**(13): p. 1654-1664.
711 75. Klose, C.S., et al., *A T-bet gradient controls the fate and function of CCR6-RORgammat+*
712 *innate lymphoid cells.* Nature, 2013. **494**(7436): p. 261-5.
713 76. Sawa, S., et al., *Lineage relationship analysis of RORgammat+ innate lymphoid cells.* Science,
714 2010. **330**(6004): p. 665-9.
715 77. Wadie, K.W., M.H. Bashir, and M.M.S. Abbass, *Epithelial-mesenchymal transition in gingival*
716 *tissues from chronic periodontitis patients: A case-control study.* Dent Med Probl, 2021. **58**(3):
717 p. 311-319.
718 78. Okawa, H., et al., *Fluorescent risedronate analogue 800CW-pRIS improves tooth extraction-*
719 *associated abnormal wound healing in zoledronate-treated mice.* Commun Med (Lond), 2022.
720 **2**: p. 112.

721

722

723 **Figure Legends**

724 **Figure 1.** Changes in proportions of major cell types during ligature-induced periodontitis
725 development in mice. (**A**) Mouse maxillary second molar (M2) has multi-roots and supported by
726 alveolar bone (Bone), periodontal ligament (PDL) and gingiva connective tissue (gCT). The oral
727 barrier immunity is not constitutively activated as evidenced by the lack of CD45+ immune cells.
728 Picrosirius red (PSR) stained collagen fibers connected the root surface and alveolar bone in the
729 PDL and organized as dense parallel bundles in gCT. (**B**) One day (Day 1) after a ligature (5.0
730 silk suture) was placed around M2, the cervical PDL and gCT demonstrated a localized
731 connective tissue degradation (*), where CD45+ immune cells clustered (arrows). PSR-stained
732 collagen architecture immediately under the ligature lost the thick collagen bundle structure (*).
733 (**C**) Day 3 of ligature placement exhibited localized but increased CD45+ immune cell clustering
734 adjacent to the collagen degradation area (*). (**D**) Day 7 of ligature placement, PDL and gCT
735 tissue degradation increased with inflammatory vascularization (Vas). CD45+ myeloid cells
736 (arrowheads) were observed near the alveolar bone surface and CD45+ lymphocytes (arrows)
737 infiltrated the gCT area. PSR staining lost the typical collagen pattern in gCT and PDL, and a
738 remnant of degraded PDL collagen fiber (white bracket) was attached to the tooth surface. (**E**)
739 Single-cell RNA sequencing (scRNA-seq) *t*-distributed stochastic neighbor embedding (*t*-SNE)
740 projection plots showing the major cell types present within gingival tissue during periodontitis
741 development on Day 0, 1, 4, and 7. Colors indicate cell type, as follows: green, epithelial cells;
742 blue, fibroblasts; pink, endothelial cells; yellow, B cells; red, T cells; and purple, myeloid cells. (**F**)
743 Proportion plots showing the relative amounts of each major cell type on Days 0, 1, 4, and 7.

744

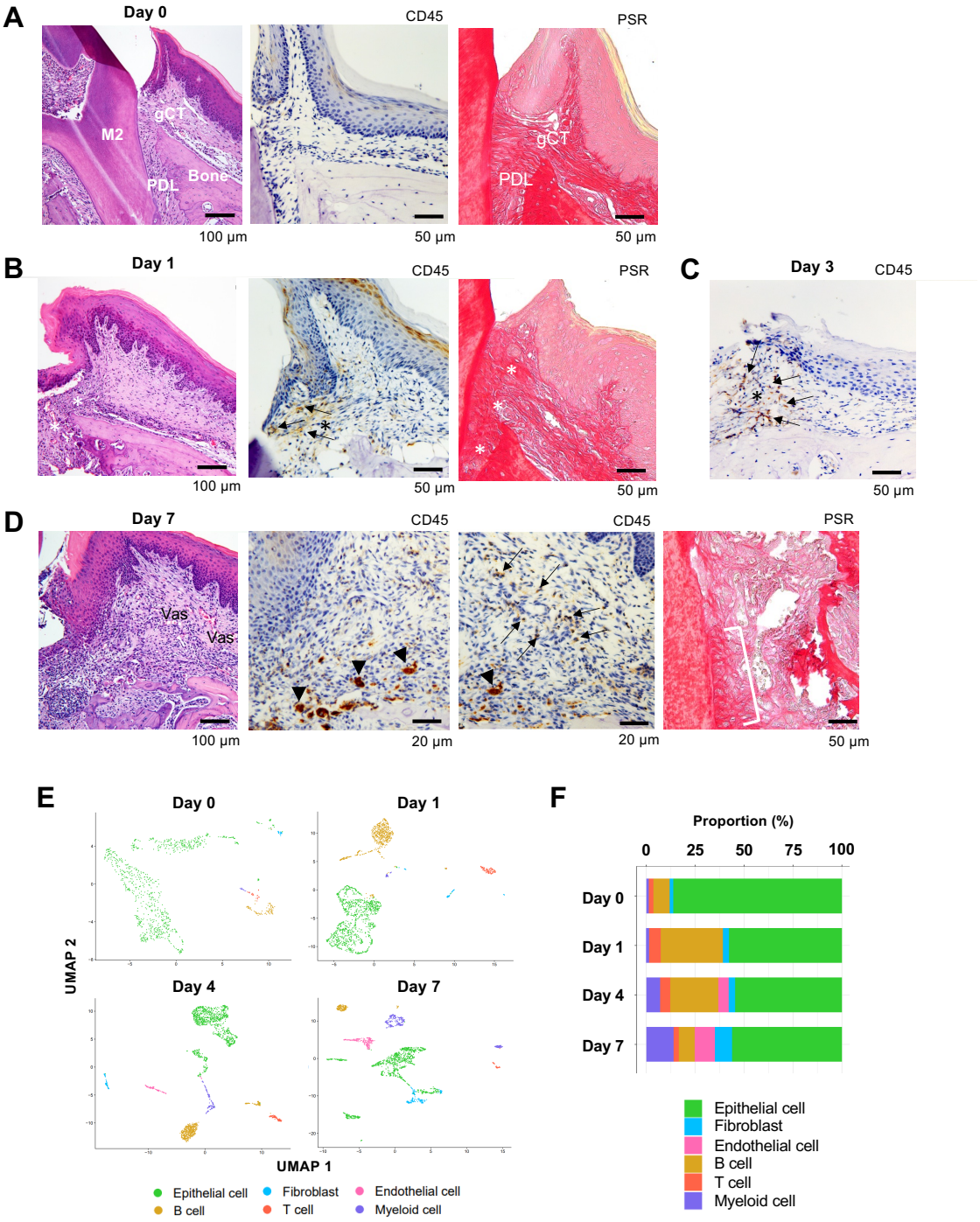
A
Day 0
CD45
PSR
M2
gCT
PDL
Bone
gCT
PDL
100 µm
50 µm
50 µm
B
Day 1
CD45
PSR
100 µm
50 µm
50 µm
C
Day 3
CD45
50 µm
D
Day 7
CD45
CD45
PSR
Vas
Vas
100 µm
20 µm
20 µm
50 µm
E
Day 0
Day 1
Day 4
Day 7
UMAP 2
UMAP 1
Epithelial cell
Fibroblast
Endothelial cell
B cell
T cell
Myeloid cell
F
Proportion (%)
0
25
50
75
100
Day 0
Day 1
Day 4
Day 7
Epithelial cell
Fibroblast
Endothelial cell
B cell
T cell
Myeloid cell

745

746

747 **Figure 2.** Fibroblasts activated to guide leukocyte migration (AG fibroblasts) are one of three
748 fibroblast subpopulations in gingival tissue during periodontitis development. (**A**) Violin plots
749 showing gene expression levels of type I collagen (*Col1a1*), type XIV collagen (*Col14a1*), and
750 smooth muscle aortic actin 2 (*Acta2*) in gingival fibroblast subpopulations during periodontitis
751 development. AG, AG fibroblasts; KT, 'keeping typical phenotype' fibroblasts; MF, myofibroblasts.
752 Gene ontology (GO) enrichment analysis of the biological functions of AG fibroblasts and KT
753 fibroblasts on Day 0 without ligature placement (**B**) and on Day 1 (**C**) and Day 7 (**D**) after ligature
754 placement. Gene clusters related to immune regulation (red) were identified in AG fibroblasts,
755 and these clusters dominate after ligature placement. (**E**) *t*-SNE projection plots showing fibroblast
756 subpopulations in gingival tissue during periodontitis development. Colors indicate cell type, as
757 follows: blue, KT fibroblasts; red, AG fibroblasts; and yellow, MFs. (**F**) Proportion plots showing
758 the relative amounts of each fibroblast subpopulation on Days 0, 1, 4, and 7.

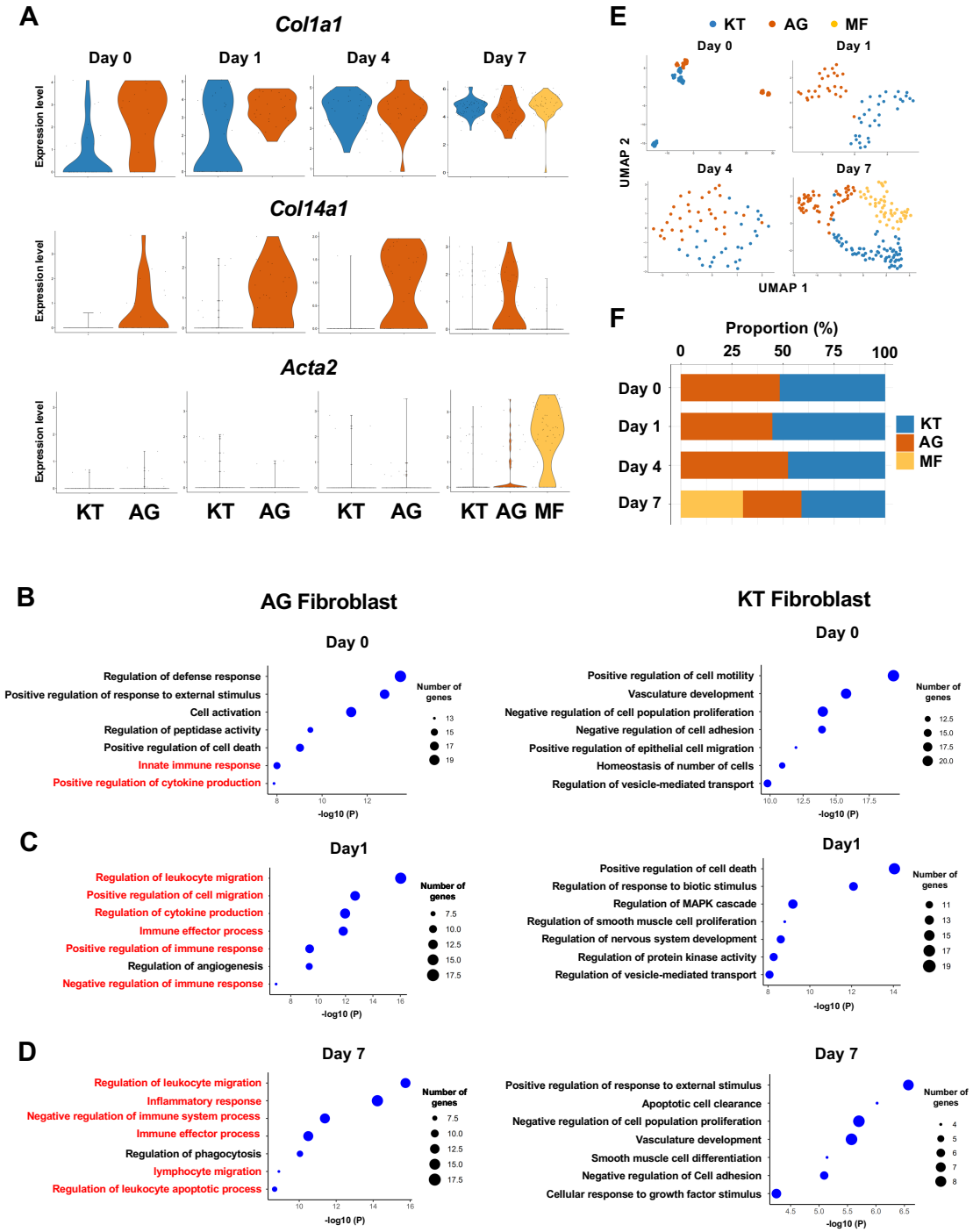
A
Col1a1
Day 0
Day 1
Day 4
Day 7
Expression level
Col14a1
Acta2
KT
AG
MF
E
UMAP 2
UMAP 1
F
Proportion (%)
0
25
50
75
100
B
AG Fibroblast
KT Fibroblast
Regulation of defense response
Positive regulation of response to external stimulus
Cell activation
Regulation of peptidase activity
Positive regulation of cell death
Innate immune response
Positive regulation of cytokine production
Number of genes
-log10 (P)
Positive regulation of cell motility
Vasculature development
Negative regulation of cell population proliferation
Negative regulation of cell adhesion
Positive regulation of epithelial cell migration
Homeostasis of number of cells
Regulation of vesicle-mediated transport
C
Day1
Regulation of leukocyte migration
Positive regulation of cell migration
Regulation of cytokine production
Immune effector process
Positive regulation of immune response
Regulation of angiogenesis
Negative regulation of immune response
Positive regulation of cell death
Regulation of response to biotic stimulus
Regulation of MAPK cascade
Regulation of smooth muscle cell proliferation
Regulation of nervous system development
Regulation of protein kinase activity
Regulation of vesicle-mediated transport
D
Day 7
Regulation of leukocyte migration
Inflammatory response
Negative regulation of immune system process
Immune effector process
Regulation of phagocytosis
lymphocyte migration
Regulation of leukocyte apoptotic process
Positive regulation of response to external stimulus
Apoptotic cell clearance
Negative regulation of cell population proliferation
Vasculature development
Smooth muscle cell differentiation
Negative regulation of Cell adhesion
Cellular response to growth factor stimulus

759

760 **Figure 3.** AG fibroblasts and immune surveillance in periodontitis development. (**A**) Dot plots
761 depicting expression levels of the CCL genes *Ccl8*, *Ccl11*, *Ccl19*, *Cxcl1*, *Cxcl9*, *Cxcl10*, and
762 *Cxcl12* in gingival fibroblast subpopulations during periodontitis development. (**B**) Dot plots
763 depicting expression levels of the Toll-like receptor and related genes *Tlr2*, *Tlr3*, *Tlr4*, *Myd88*,
764 *Irak1*, *Map3k7*, and *Rela* in gingival fibroblast subpopulations during periodontitis development.
765 Upregulation of chemokines and TLR-related molecules is predominantly observed in the AG
766 fibroblast subpopulation. (**C**) Hematoxylin and eosin (HE) staining and immunohistochemical
767 (IHC) staining for COL14A1 and CXCL12 in periodontal tissue on Day 1; scale bars, 100 μm (HE)
768 and 20 μm, (IHC). Yellow arrows indicate COL14A1- and CXCL12-positive cells in the connective
769 tissue papillae and periodontal ligament (PDL).

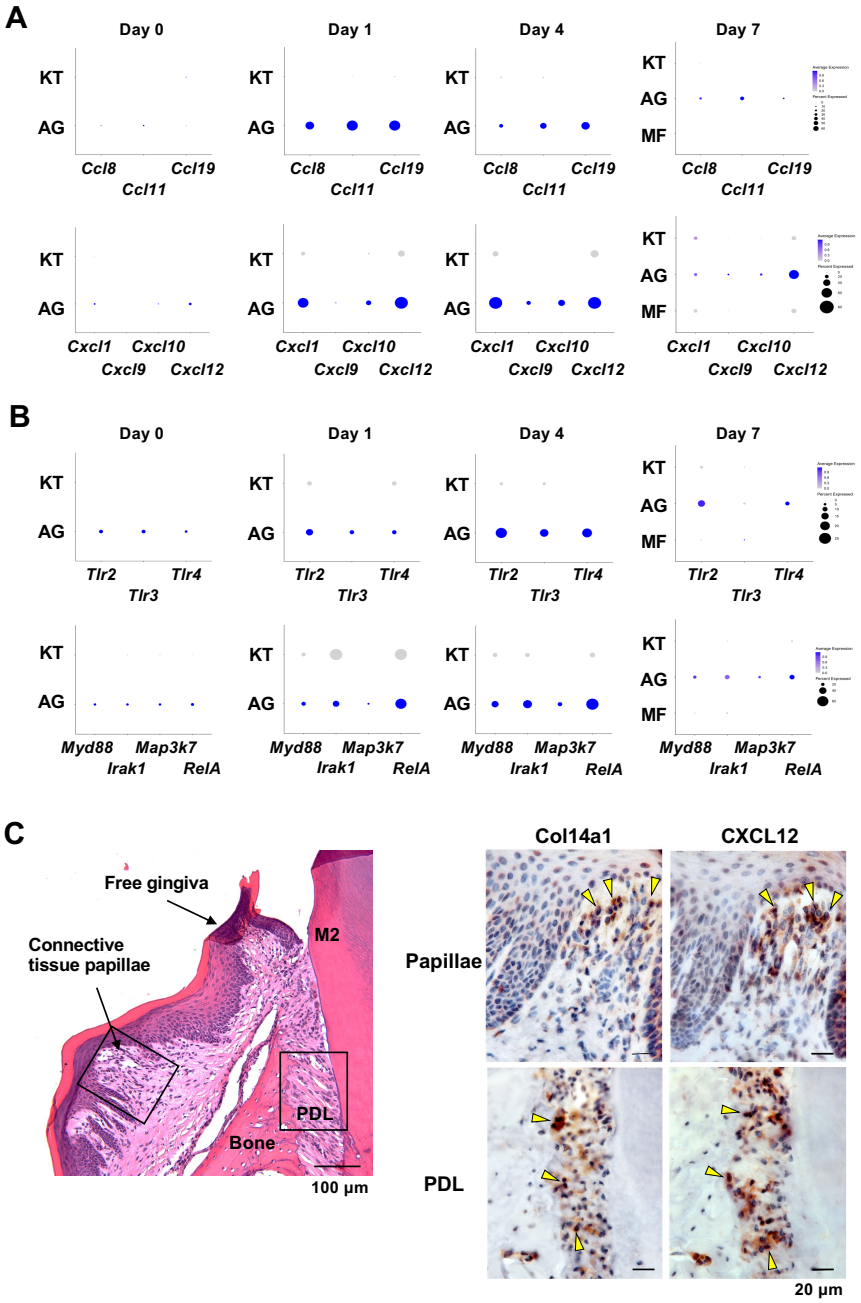
A
Day 0
Day 1
Day 4
Day 7
KT
AG
MF
Ccl8
Ccl19
Ccl11
Cxcl1
Cxcl10
Cxcl9
Cxcl12
B
Tlr2
Tlr4
Tlr3
Myd88
Map3k7
Irak1
RelA
C
Free gingiva
Connective tissue papillae
M2
PDL
Bone
100 µm
Col14a1
CXCL12
Papillae
PDL
20 µm

770

771 **Figure 4.** Characterization of AG fibroblasts in the discrete maxillary topical application (MTA)
772 model using CpG ODN (TLR9 ligand) and LPS (TLR2/4 ligand). (**A**) The MTA model was
773 developed to discretely test the selected oral microbial pathogens. The selected pathogen was
774 topically applied directly on the maxillary gingiva between the molars and covered by a custom
775 fabricated oral appliance for 1 hr. (**B**) In this study, microbial DNA TLR9 ligand, unmethylated
776 CpG ODN and TLR2/4 ligand *P. gingivalis* lipopolysaccharide (LPS) were selected in the MTA
777 model. After 1 hr exposure, mice were returned to the vivarium for 4 days and the maxillary tissue
778 was harvested for histology or scRNA-seq. (**C**) The MTA of CpG ODN developed localized PDL
779 and gCT degradation evidenced by the expression of cathepsin K (Ctsk; arrows). There were
780 signs of localized bone resorption by Ctsk+ osteoclasts (arrowheads) on the surface of alveolar
781 bone (Bone). (**D**) Gingival cell composition by scRNA-seq of the MTA of CpG ODN or LPS
782 revealed early stage of gingival inflammation, equivalent to Day 1 of the ligature-induced
783 periodontitis model. (**E**) The fibroblastic gene expression signature revealed the presence of KT
784 and AG fibroblasts by the MTA of CpG ODN, whereas the MTA of LPS induced MF. (**F**) AG
785 fibroblasts of the MTA of CpG ODN and LPS were activated to express CCL and CXCL
786 chemokines. (**G**) The MTA of CpG ODN did not upregulate *Tlr9*, whereas the MTA of LPS
787 increased the expression of *Tlr2/4* in AG fibroblasts. However, the both the MTA of CpG ODN
788 and LPS increased the expression of TLR downstream molecules.

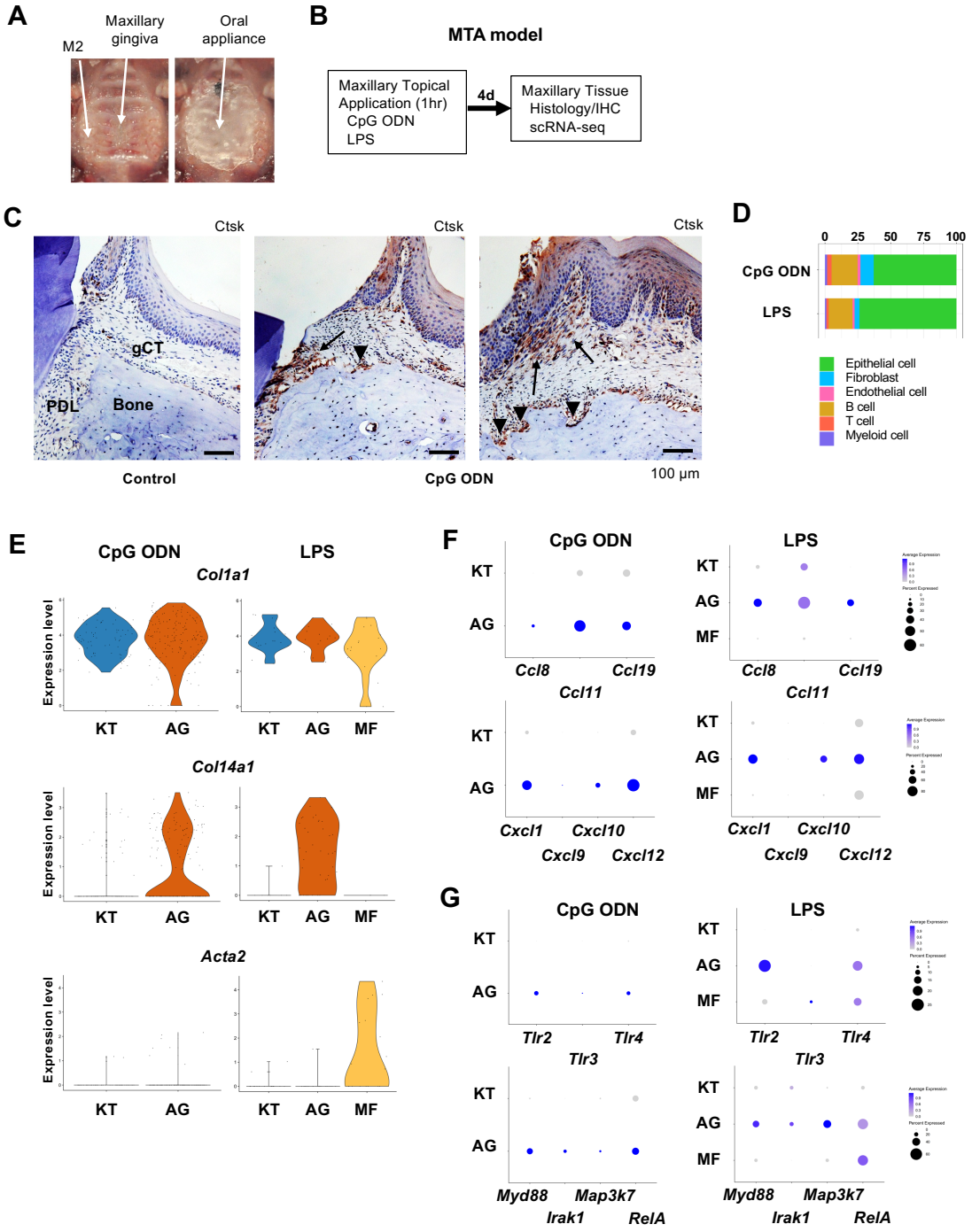
A
M2
Maxillary gingiva
Oral appliance
B
MTA model
Maxillary Topical Application (1hr)
CpG ODN
LPS
4d
Maxillary Tissue
Histology/IHC
scRNA-seq
C
Ctsk
gCT
PDL
Bone
Control
CpG ODN
100 µm
D
0
25
50
75
100
CpG ODN
LPS
Epithelial cell
Fibroblast
Endothelial cell
B cell
T cell
Myeloid cell
E
CpG ODN
LPS
Col1a1
Col14a1
Acta2
Expression level
KT
AG
MF
F
CpG ODN
LPS
Ccl8
Ccl19
Ccl11
Cxcl1
Cxcl10
Cxcl9
Cxcl12
G
Tlr2
Tlr4
Tlr3
Myd88
Map3k7
Irak1
RelA

789

790 **Figure 5.** Myeloid cell composition and activity in gingival tissue during in periodontitis
791 development. (**A**) *t*-SNE projection plots showing myeloid cell subpopulations in gingival tissue
792 during periodontitis development on Days 0, 1, 4, and 7. Colors indicate cell type, as follows:
793 green, macrophages and red, neutrophils. (**B**) Proportion plots showing the relative amounts of
794 neutrophils and macrophages on Days 0, 1, 4, and 7. (**C**) Violin plots showing *Trem1* and *Mmp9*
795 expression levels in myeloid cells on Days 0, 1, 4, and 7; both genes are upregulated in
796 neutrophils after ligature placement. (**D**) Violin plots showing *Tgfb1* and *Tnf* expression in myeloid
797 cells on Days 0, 1, 4, and 7; no obvious induction is observed in response to ligature placement.
798 (**E**) Dot plots depicting expression levels of the C motif chemokine ligand (CCL) genes *Ccl2*, *Ccl3*,
799 *Ccl4*, *Ccl6*, *Ccl9*. (**F**) The expression of CXC motif chemokine ligand (CXCL) genes *Cxcl2*, *Cxcl3*,
800 *Cxcl4,* and *Cxcl9*. Chemokine expression in myeloid cells was unrelated to progression of gingival
801 inflammation from Day 1 to 7.

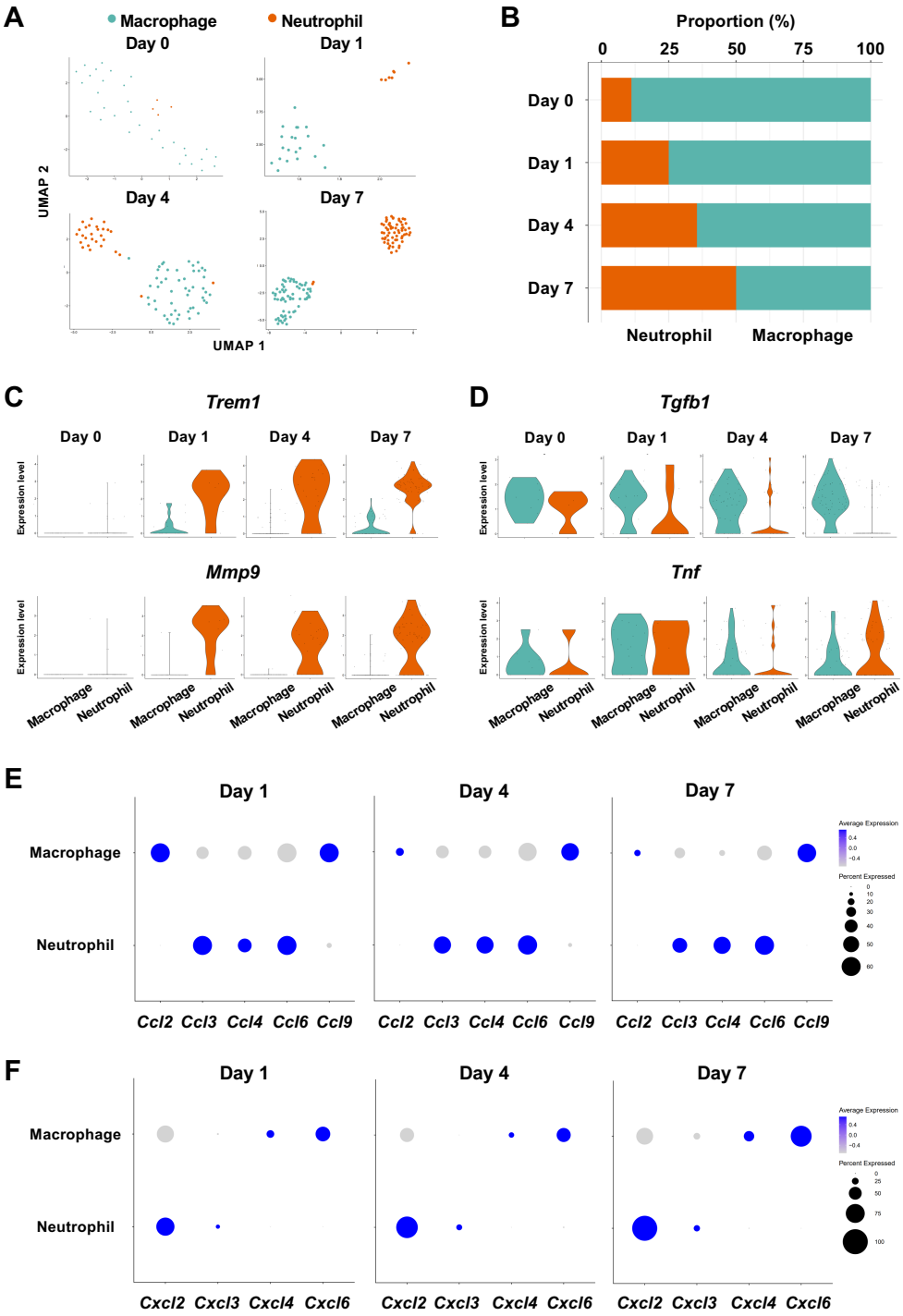
A
Macrophage
Neutrophil
Day 0
Day 1
Day 4
Day 7
UMAP 2
UMAP 1
B
Proportion (%)
0
25
50
75
100
Day 0
Day 1
Day 4
Day 7
Neutrophil
Macrophage
C
Trem1
Mmp9
Day 0
Day 1
Day 4
Day 7
Expression level
Macrophage
Neutrophil
D
Tgfb1
Tnf
E
Day 1
Day 4
Day 7
Macrophage
Neutrophil
Ccl2 Ccl3 Ccl4 Ccl6 Ccl9
Average Expression
Percent Expressed
F
Cxcl2 Cxcl3 Cxcl4 Cxcl6

802

803 **Figure 6.** Role of AG fibroblasts in myeloid cell activation. (**A**) Interaction between chemokine
804 ligands expressed by AG fibroblasts and their putative chemokine receptors expressed by
805 myeloid cells during periodontitis development. Dot plots depicting expression levels of the CC
806 chemokine receptor (CCR) and the CXC chemokine receptor (CXCR) genes *Ccr1*, *Ccr2*, *Ccr5*,
807 *Ccr7*, *Cxcr2*, *Cxcr3*, and *Cxcr4* in myeloid cell subpopulations on Day 1 and Day 7 following
808 ligature placement. (**B**) NicheNet ligand–target matrix indicating the regulatory potential between
809 active ligands expressed in fibroblasts and target genes expressed in myeloid cells from the p-
810 EMT program on Day 1 and Day 7. (**E**) Dot plot depicting expression levels of active ligand genes
811 from panel (**B**) in fibroblast subpopulations on Day 1 and Day 7. (**D**) Dot plot depicting expression
812 levels of target genes from panel (**B**) in myeloid cell subpopulations on Day 1 and Day 7. Results
813 suggest a strong intercellular communication network from AG fibroblasts to neutrophils. (**E**)
814 Interaction between chemokine ligands expressed by AG fibroblasts and their putative chemokine
815 receptors expressed by myeloid cells in the MTA model of CpG ODN and LPS.

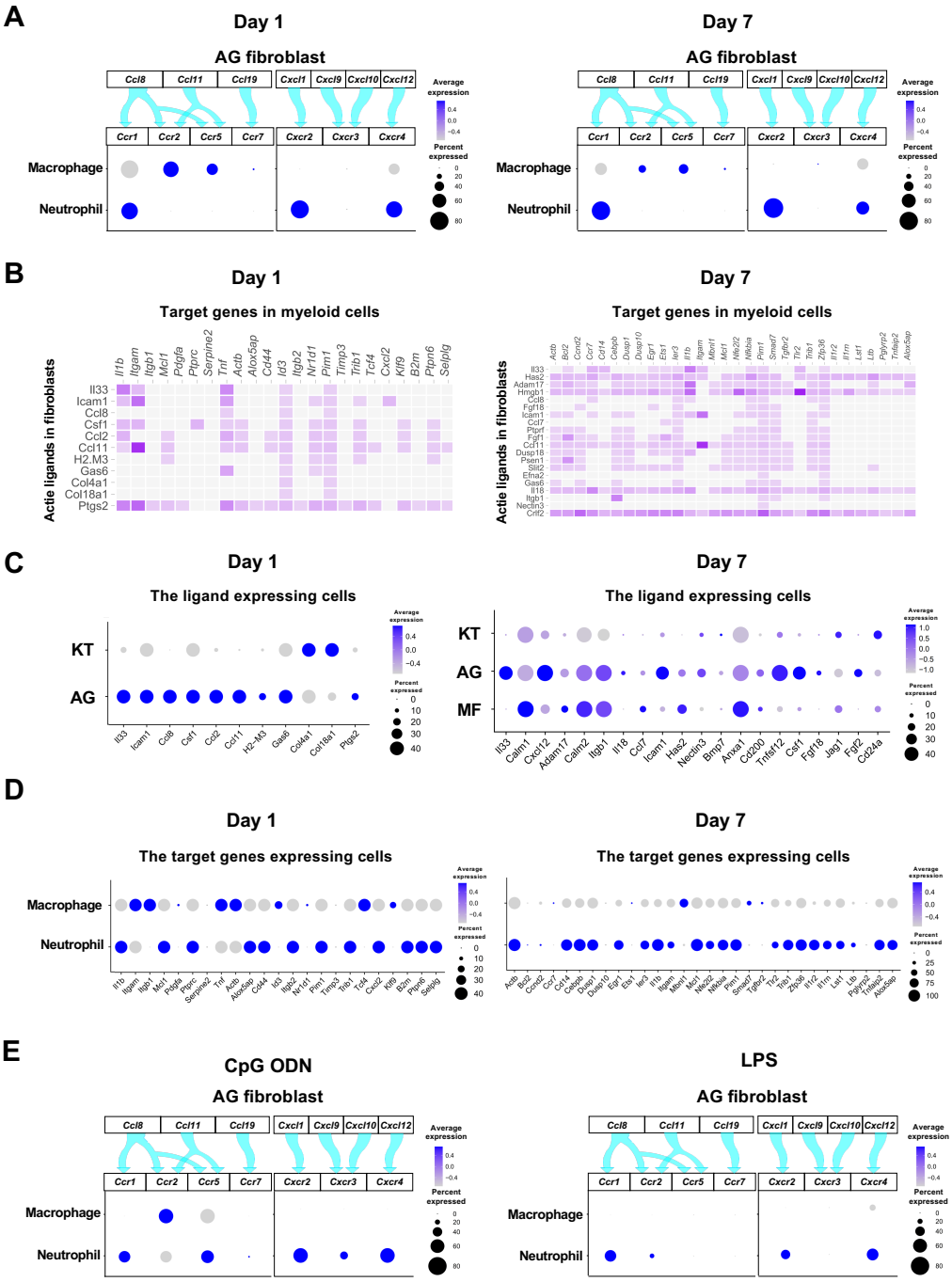
A
Day 1
AG fibroblast
Ccl8
Ccl11
Ccl19
Cxcl1
Cxcl9
Cxcl10
Cxcl12
Ccr1
Ccr2
Ccr5
Ccr7
Cxcr2
Cxcr3
Cxcr4
Macrophage
Neutrophil
Average expression
Percent expressed
Day 7
AG fibroblast
B
Day 1
Target genes in myeloid cells
Actie ligands in fibroblasts
Il1b
Itgam
Itgb1
Mcl1
Pdgfa
Ptprc
Serpine2
Tnf
Actb
Alox5ap
Cd44
Id3
Itgb2
Nr1d1
Plm1
Timp3
Trib1
Tcf4
Cxcl2
Klf9
B2m
Ptpn6
Selplg
Il33
Icam1
Ccl8
Csf1
Ccl2
Ccl11
H2.M3
Gas6
Col4a1
Col18a1
Ptgs2
Day 7
Target genes in myeloid cells
C
Day 1
The ligand expressing cells
KT
AG
Day 7
The ligand expressing cells
KT
AG
MF
D
Day 1
The target genes expressing cells
Macrophage
Neutrophil
Day 7
The target genes expressing cells
E
CpG ODN
AG fibroblast
LPS
AG fibroblast

816

817 **Figure 7.** The cellular source of osteoclastogenic cytokines: M-CSF and RANKL in the ligature-
818 induced model and the MTA model. (**A**) Violin plots showing expression levels of the macrophage-
819 colony stimulating factor (M-CSF)-encoding gene, *Csf1* (M-CSF), in each major cell type from the
820 ligature-induced periodontitis model. (**B**) Violin plots showing expression levels of *Csf1* in
821 fibroblast subpopulations, myeloid cell subpopulations, and T cell subpopulations. (**C**) Violin plots
822 showing expression levels of the nuclear factor kappa-B ligand (RANKL)-encoding gene, *Tnfsf11,*
823 in each major cell type. (**D**) Violin plots showing expression levels of *Tnfsf11* in fibroblast
824 subpopulations, myeloid cell subpopulations, and T cell subpopulations. (**E**) Violin plots of *Csf1*
825 expressing cells in the MTA model. (**F**) Violin plots of *Tnfsf11*expressing cells in the MTA model.
826 AG fibroblasts predominantly expressed *Tnfsf11*.

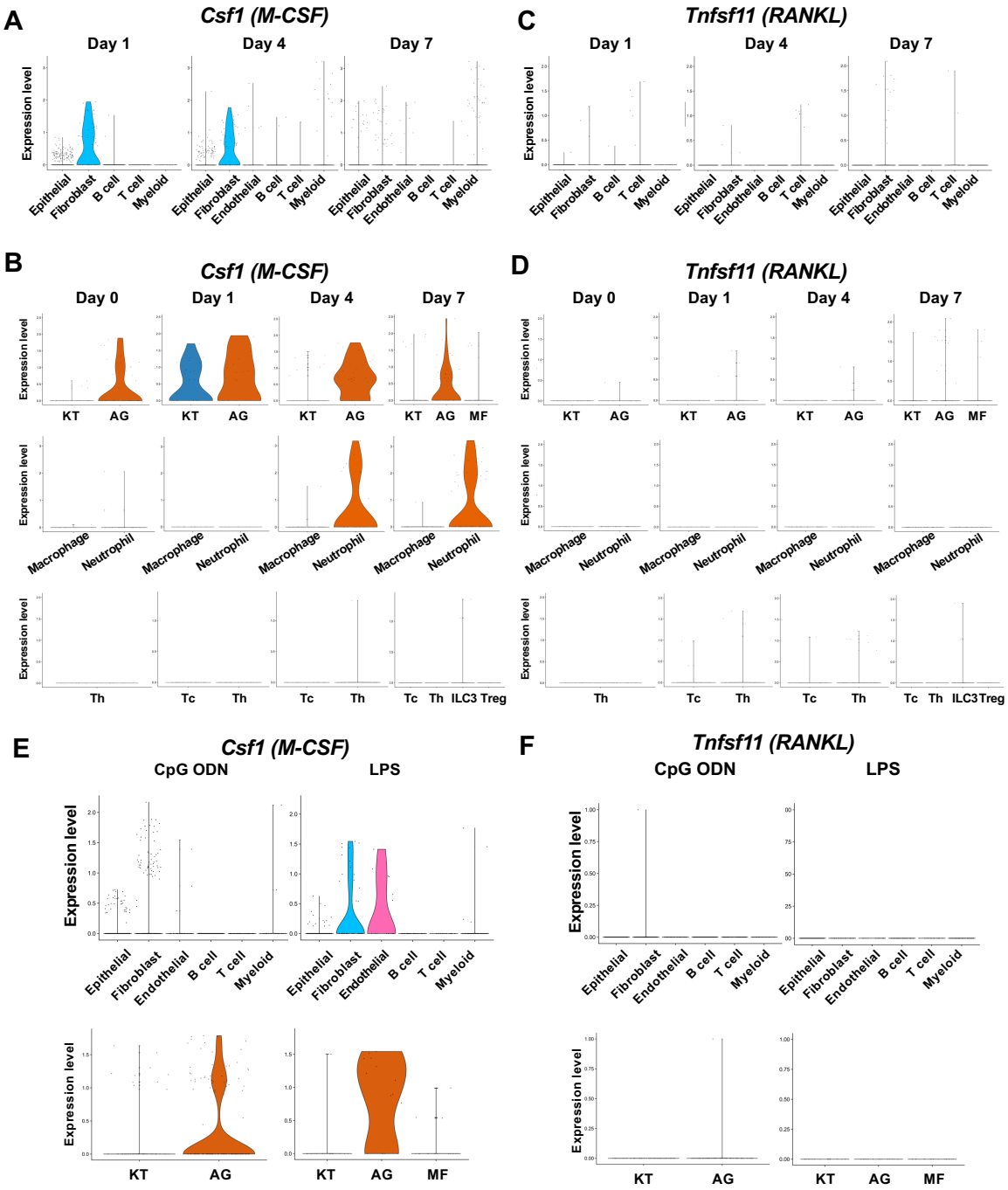
A
Csf1 (M-CSF)
Day 1
Day 4
Day 7
Expression level
Epithelial
Fibroblast
B cell
T cell
Myeloid
Endothelial
C
Tnfsf11 (RANKL)
B
Day 0
KT
AG
MF
Macrophage
Neutrophil
Th
Tc
ILC3
Treg
D
E
CpG ODN
LPS
F

827

828 **Figure 8.** ILC3s are critical for cervical alveolar bone resorption in the ligature-induced
829 periodontitis development. (**A**) Proportion plots showing the relative amounts of T cell
830 subpopulations in gingival tissue during periodontitis development. Treg, T regulatory cells; ILC,
831 innate lymphoid cells; Th, T helper cells; Tc, cytotoxic T cells. (**B**) Violin plots showing
832 expression levels of the T cell marker genes *Cd8* (Tc), *Cd4* (Th), *Zbtb16* (ILC), and *Foxp3*
833 (Treg) on Day 7 following ligature placement. (**C**) Violin plots showing expression levels of *Nfil3*,
834 *Rorγ*, *Il17a*, *Il17f*, *Tbx21*, and *Gata3* on Day 7 following ligature placement. These gene
835 signatures indicate that gingival ILCs primarily comprise type 3 ILCs (ILC3s). (**D**) Representative
836 microCT images of the maxilla taken from the lateral view for the ligated side and from the
837 contralateral view for the unligated side. (**E**) Alveolar bone loss was determined from the total
838 distance between the CEJ and the ABC of the buccal bone or palatal bone at six sites in the
839 ligated side (n = 6). (**F**) HE staining of the periodontal tissue on Day 7. gCT, gingival connective
840 tissue; Bone, alveolar bone; PDL, periodontal ligament; scale bars, 100 μm. (**G**) Tartrate-
841 resistant acid phosphatase (TRAP) staining of periodontal tissue from WT mice on Day 7; scale
842 bar, 100 μm. Total number of TRAP-positive cells in a 0.01 mm^2-area of the buccal and palatal
843 bone in the cervical PDL site (**H**) and apical PDL site (**H**) (n = 6). Significance was determined
844 by ANOVA, with Tukey's multiple-comparison test. Data are presented as mean values ± SD; p
845 < 0.05 was considered significant.

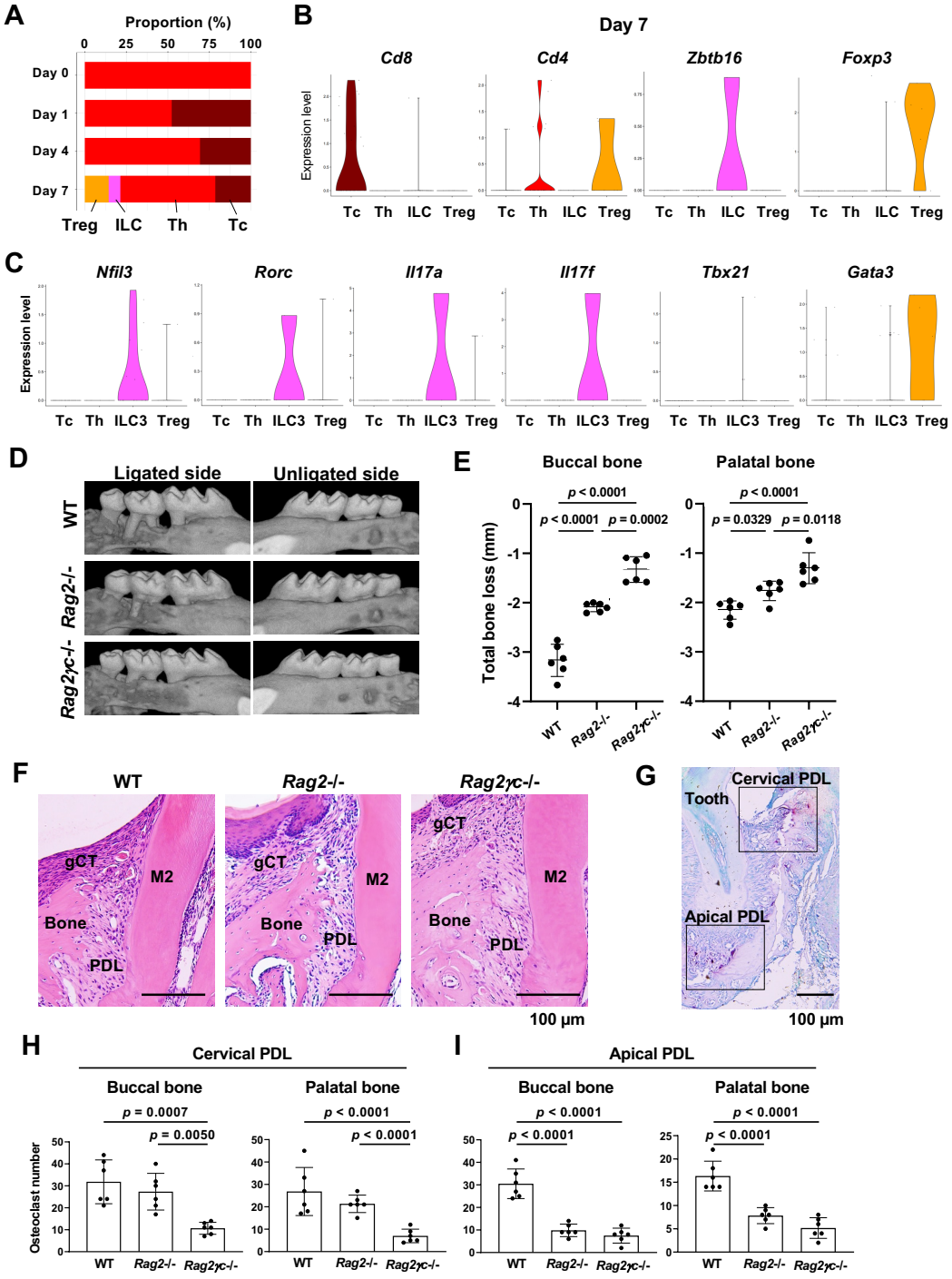
A
Proportion (%)
0 25 50 75 100
Day 0
Day 1
Day 4
Day 7
Treg ILC Th Tc
B
Day 7
Cd8
Cd4
Zbtb16
Foxp3
Expression level
Tc Th ILC Treg
C
Nfil3
Rorc
Il17a
Il17f
Tbx21
Gata3
Expression level
Tc Th ILC3 Treg
D
Ligated side
Unligated side
WT
Rag2-/-
Rag2γc-/-
E
Buccal bone
Palatal bone
Total bone loss (mm)
p < 0.0001
p < 0.0001
p = 0.0002
p < 0.0001
p = 0.0329
p = 0.0118
WT
Rag2-/-
Rag2γc-/-
F
WT
Rag2-/-
Rag2γc-/-
gCT
M2
Bone
PDL
100 μm
G
Cervical PDL
Tooth
Apical PDL
100 μm
H
Cervical PDL
Buccal bone
Palatal bone
Osteoclast number
p = 0.0007
p = 0.0050
p < 0.0001
p < 0.0001
WT
Rag2-/-
Rag2γc-/-
I
Apical PDL
Buccal bone
Palatal bone
p < 0.0001
p < 0.0001
p < 0.0001
p < 0.0001
WT
Rag2-/-
Rag2γc-/-

846

847 **Figure 9.** The role of AG fibroblasts and neutrophils in ILC3 development in periodontitis. Violin
848 plots showing expression levels of the genes encoding interleukin (IL)-6 (*Il6)* (**A**) and IL-23 *(Il23a)*
849 (**B**) in each major cell type, fibroblast subpopulations, and myeloid cell subpopulations during
850 periodontitis development. (**C**) Interaction between chemokine ligands strongly expressed by AG
851 fibroblasts and their putative chemokine receptors expressed by T cells, including ILCs. Dot plots
852 depict gene expression levels of *Ccr1*, *Ccr2*, *Ccr5*, *Ccr7*, *Ccr8*, *Cxcr2*, *Cxcr3*, and *Cxcr4* in T cell
853 subpopulations on Day 7 following ligature placement. (**D**) Interaction between chemokine ligands
854 strongly expressed by neutrophils and their putative chemokine receptors expressed by T cells.
855 Dot plots depicting gene expression levels of *Ccr1*, *Ccr4*, and *Ccr5* in T cell subpopulations on
856 Day 7 following ligature placement. (**E**) NicheNet ligand–target matrix denoting the regulatory
857 potential between active ligands in fibroblasts and target genes in T cells from the p-EMT program
858 on Day 7 following ligature placement. (**F**) NicheNet ligand–target matrix denoting the regulatory
859 potential between active ligands in myeloid cells and target genes in T cells from the p-EMT
860 program on Day 7 following ligature placement. (**G**) Dot plot depicting expression levels of active
861 ligand genes from panel (**E**) in fibroblast subpopulations. (**H**) Dot plot depicting expression levels
862 of active ligand genes from panel (**F**) in myeloid cell subpopulations. (**I**) Dot plot depicting
863 expression levels of target genes from pane (**E**) in T cell subpopulations. (**J**) Dot plot depicting
864 expression levels of target genes from panel (**F**) in T cell subpopulations.

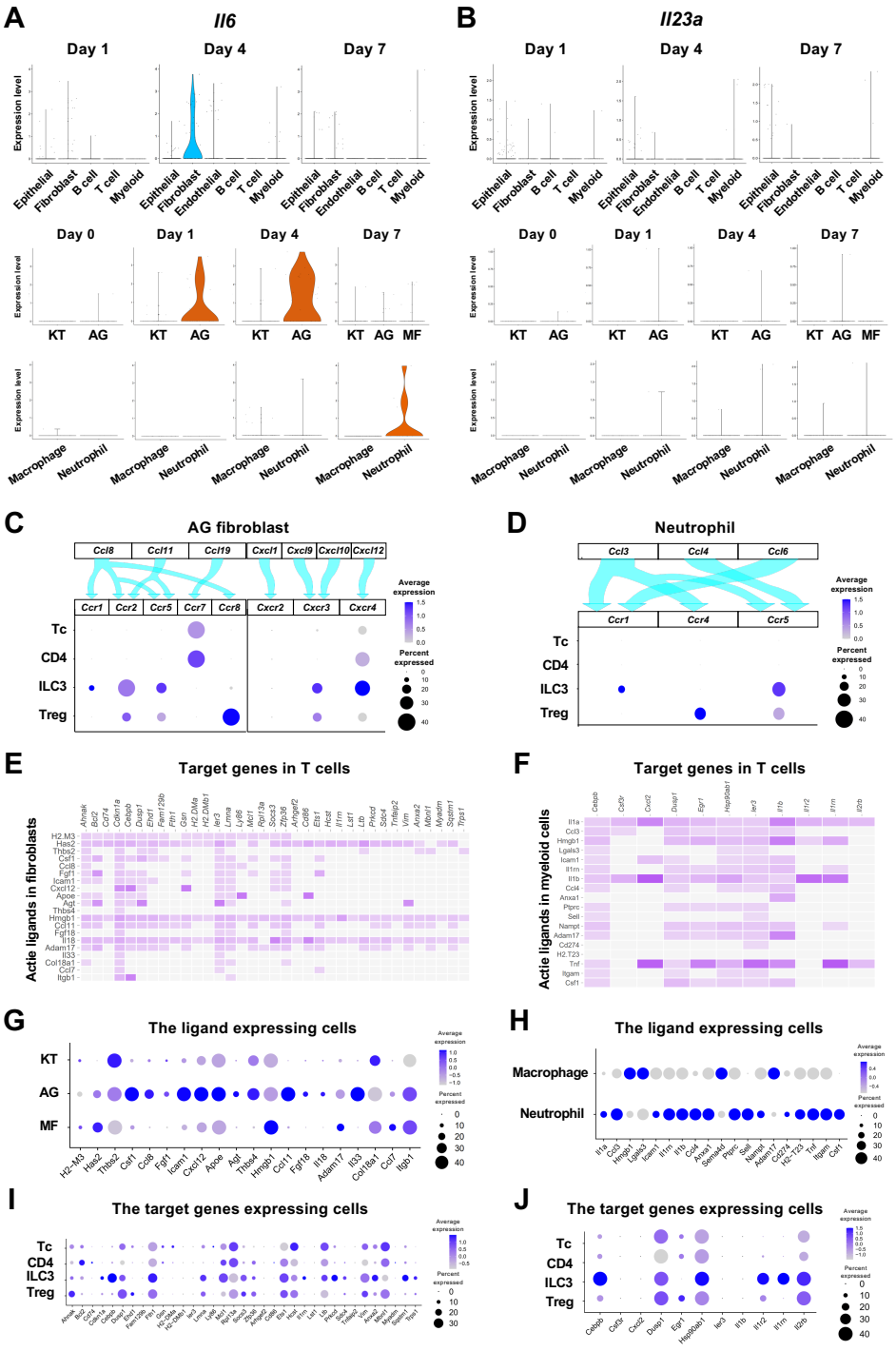
A
Il6
Day 1
Day 4
Day 7
Expression level
Epithelial
Fibroblast
B cell
T cell
Myeloid
Endothelial
Day 0
KT
AG
MF
Macrophage
Neutrophil
B
Il23a
C
AG fibroblast
Ccl8
Ccl11
Ccl19
Cxcl1
Cxcl9
Cxcl10
Cxcl12
Ccr1
Ccr2
Ccr5
Ccr7
Ccr8
Cxcr2
Cxcr3
Cxcr4
Tc
CD4
ILC3
Treg
Average expression
Percent expressed
D
Neutrophil
Ccl3
Ccl4
Ccl6
Ccr1
Ccr4
Ccr5
E
Target genes in T cells
Actie ligands in fibroblasts
F
Target genes in T cells
Actie ligands in myeloid cells
G
The ligand expressing cells
H
The ligand expressing cells
Macrophage
Neutrophil
I
The target genes expressing cells
J
The target genes expressing cells

865

866 **Figure 10.** Schematic overview of the newly proposed AG fibroblast–neutrophil–ILC3 axis. We
867 propose that periodontal inflammation is initiated by the activation of AG fibroblasts, which secrete
868 chemokines and cytokines that recruit neutrophils to sites of tissue damage. Activated neutrophils
869 and AG fibroblasts, in turn, activate ILC3s, leading to production of proinflammatory IL-17
870 cytokines. Ultimately, cervical alveolar bone resorption is facilitated by a localized
871 osteoclastogenic environment, induced by activated ILC3s, together with AG fibroblasts,
872 neutrophils, myofibroblasts, and gingival epithelial cells, including those with an epithelial–
873 mesenchymal transition (EMT) phenotype.

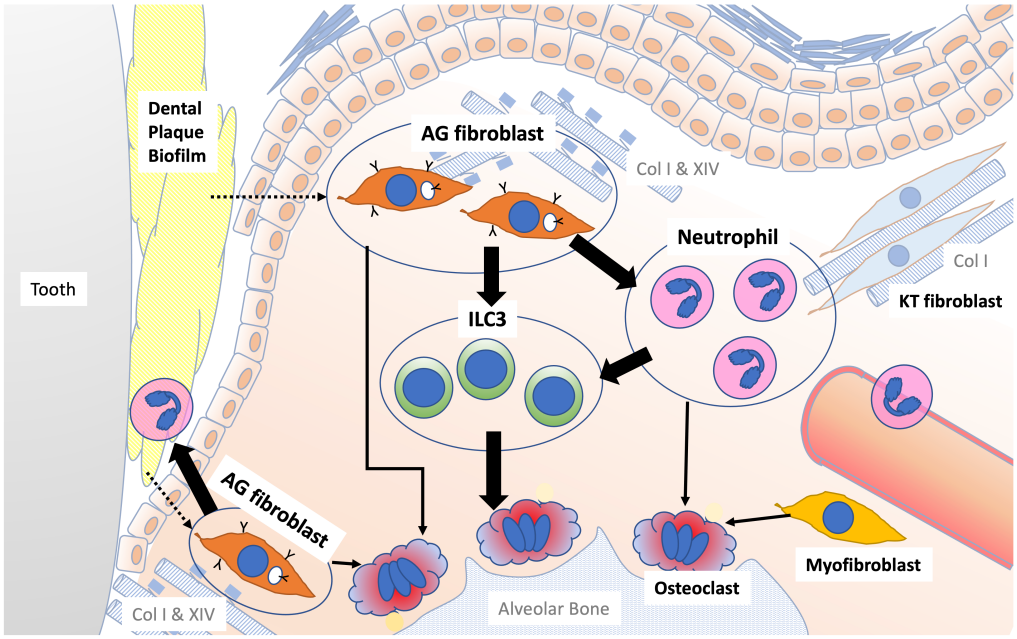
Dental
Plaque
Biofilm
AG fibroblast
Col I & XIV
Neutrophil
Col I
KT fibroblast
Tooth
ILC3
AG fibroblast
Myofibroblast
Osteoclast
Alveolar Bone
Col I & XIV

874

875

876 **Supplemental Information**

877 **Figure supplement 1. (A)** A ligature (5.0 silk suture) was placed around the maxillary second
878 molar (M2) of wild-type (WT) mice. Representative intra-oral photographs of the maxilla on Day
879 0, prior to ligature placement (healthy gingiva), and on Days 1, 3, and 7 after ligature placement.
880 (**B**) The gingival defect area was measured and normalized to the circumferential area of the
881 maxillary first molar (M1) (n = 6). Gingival defects appeared on Day 3. (**C**) Representative micro-
882 computed tomography (microCT) images of the maxilla taken from the lateral view. (**D**) Alveolar
883 bone loss was determined from the total distance between the cementoenamel junction (CEJ)
884 and the alveolar bone crest (ABC) of the buccal or palatal bone at six sites in the ligated side (n
885 = 6). Alveolar bone loss was apparent on Day 7. (**E**) Alveolar bone loss was assessed at the
886 mesiobuccal cusp (M1-1), distobuccal cusp (M1-2), and distal cusp (M1-3) of the first molar, the
887 mesiobuccal cusp (M2-1) and distobuccal cusp (M2-2) of the second molar, and the buccal cusp
888 (M3) of the third molar by measuring the distance from the cementoenamel junction (CEJ) to the
889 alveolar bone crest (ABC) on the buccal or palatal side of the alveolar bone (n = 6). Significance
890 was determined by one-way analysis of variance (ANOVA), with Tukey's multiple-comparison test.
891 Data are presented as mean values ± standard deviation (SD); $p < 0.05$ was considered
892 significant.

Figure supplement 1

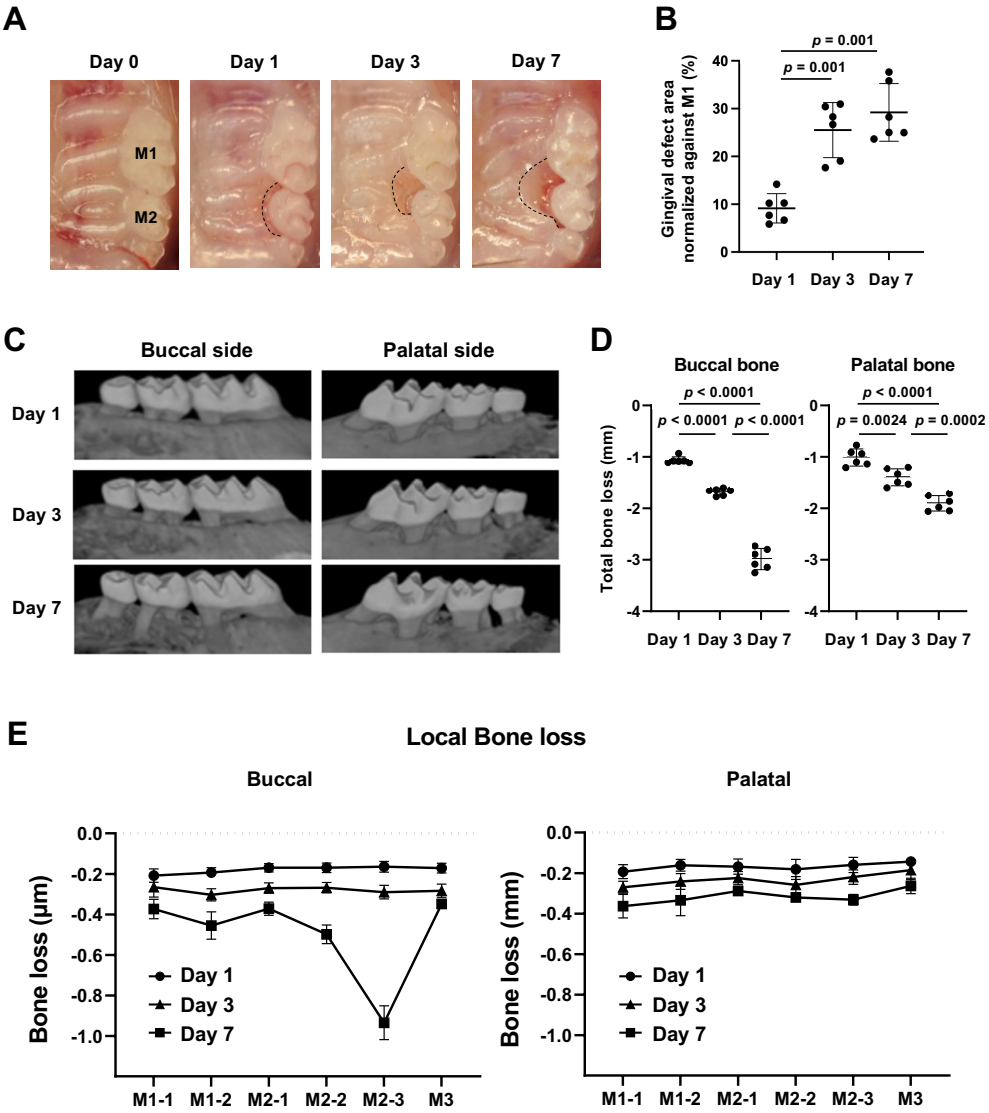

893

894 **Figure supplement 2.** Identification of major cell types in mouse gingival tissue during
895 periodontitis development by single-cell RNA sequencing (scRNA-seq). Violin plots showing
896 expression levels of cell-type marker genes in each major cell type: epithelial cells, cadherin 1
897 (*Cdh1*) and type XVII collagen (*Col17a1*); fibroblasts, type I collagen (*Col1a1*) and lumican (*Lum*);
898 endothelial cells, selectin P (*Selp*) and selectin E (*Sele*); B cells, membrane spanning 4 domains
899 A1 (*Ms4a1*) and cluster of differentiation 79A (*Cd79a*); T cells, epsilon subunit of T cell receptor
900 complex (*Cd3e*) and cluster of differentiation 5 (*Cd5*); and myeloid cells, lysozyme 2 (*Lyz2*) and
901 integrin subunit alpha M (*Itgam*).

Figure supplement 2

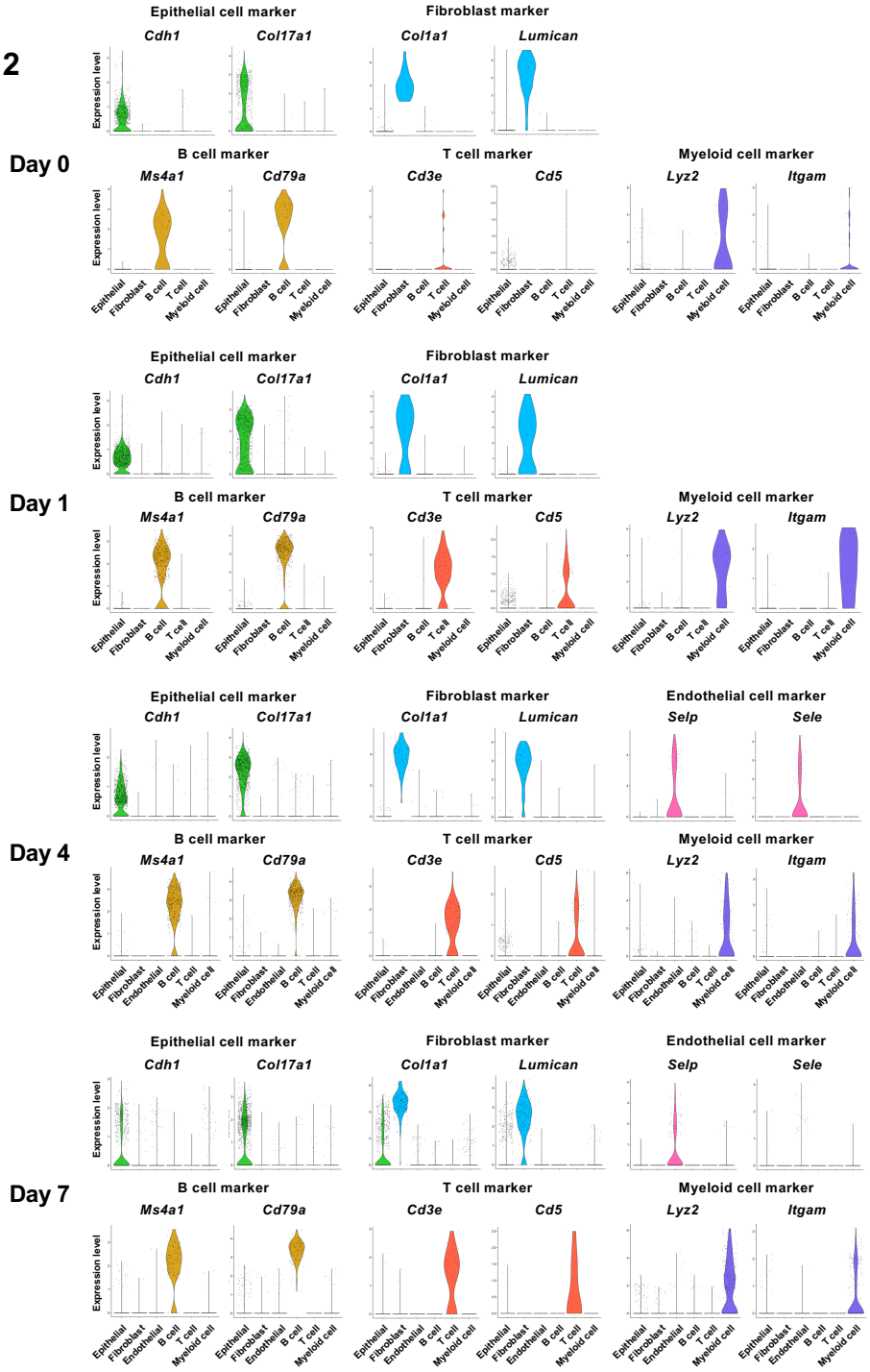

902

903 **Figure supplement 3.** Identification of myeloid cell subpopulations in mouse gingival tissue
904 during periodontitis development by scRNA-seq. Violin plots showing expression levels of
905 macrophage and neutrophil marker genes in myeloid cell subpopulations: macrophages, cluster
906 of differentiation 86 (*Cd86*) and integrin subunit alpha X (*Itgax*); and neutrophils, CXC motif
907 chemokine receptor 2 (*Cxcr2*) and G0/G1 switch gene 2 (*G0s2*).

Figure supplement 3

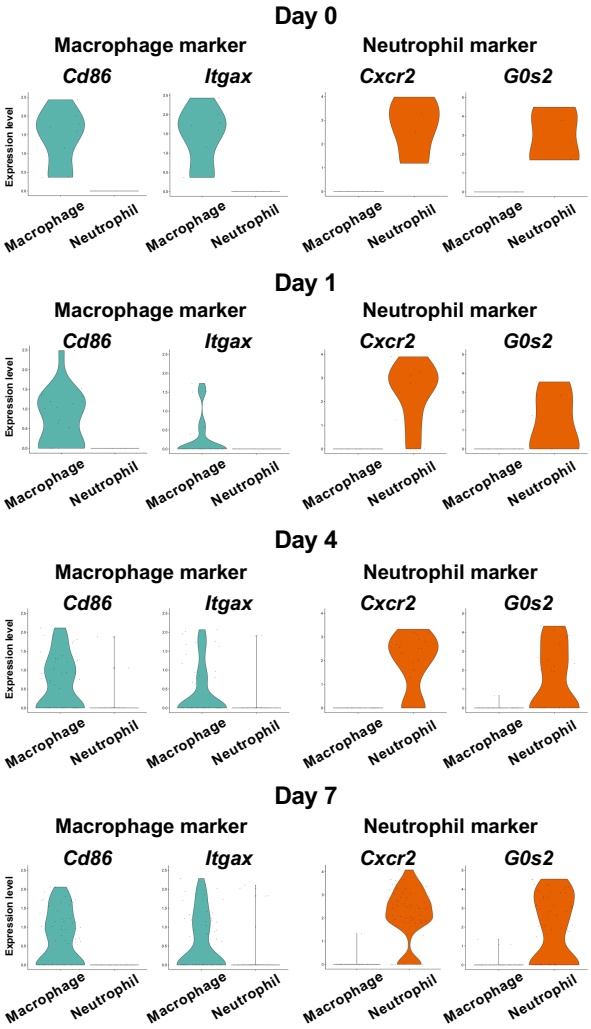

908

909 **Figure supplement 4.** Effects of innate lymphoid cell (ILC) deletion on alveolar bone loss in the
910 mouse periodontitis model. (**A**) Alveolar bone loss was assessed at six sites by measuring the
911 distance from the CEJ to the ABC on the buccal or palatal side of the alveolar bone of wild-type
912 (WT), Rag2$^{-/-}$, and Rag2$^{-/-}$γc$^{-/-}$ mice on Day 7 following ligature placement (n = 6). (**B**) Bone
913 volume/total volume (BV/TV), bone surface, trabecular number (Tb.N), and trabecular thickness
914 (Tb.Th) in the buccal side of alveolar bone of the second molar were measured on Day 7 (n = 6).
915 (**C**) Representative intra-oral photographs of maxilla from WT, Rag2$^{-/-}$, and Rag2$^{-/-}$γc$^{-/-}$ mice taken
916 on Day 7 following ligature placement. (**D**) The gingival defect area was measured and normalized
917 to the circumferential area of M1 (n = 5). Significance was determined by ANOVA, with Tukey's
918 multiple-comparison test. Data are presented as mean values ± SD; $p < 0.05$ was considered
919 significant. (**E**) Panoramic radiograph of a human patient diagnosed with generalized periodontitis.
920 The alveolar bone resorption was only noted at the cervical alveolar bone (arrows), whereas the
921 apical alveolar bone was well maintained and not affected by periodontitis. (**F**) Periapical dental
922 radiograph and the clinical pictures during the periodontal surgery. A localized alveolar bone loss
923 (arrows) was noted at the cervical periodontal ligament area.

Figure supplement 4

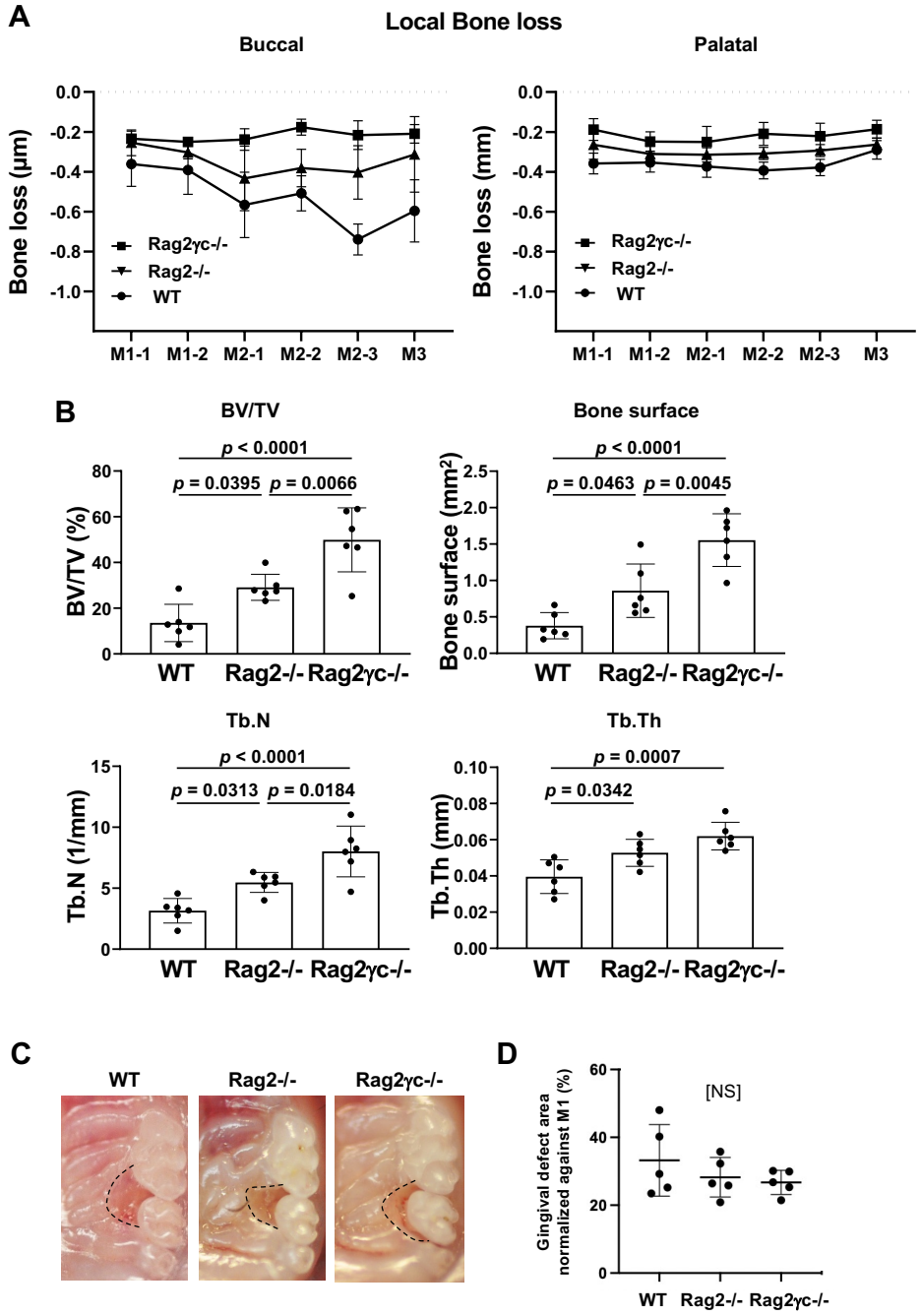

924

Figure supplement 4

E

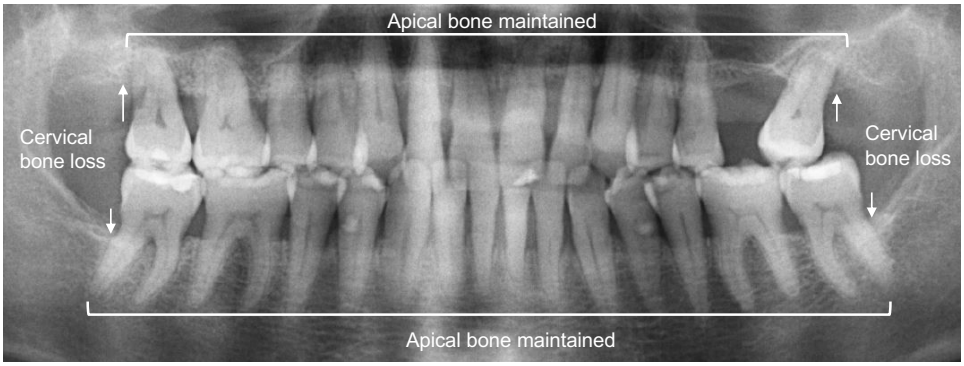

F

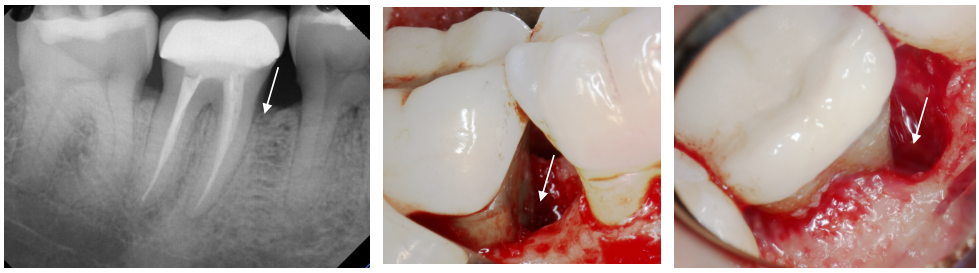

925

926 **Figure supplement 5.** Epithelial cell subpopulations involved in periodontitis development in mice.
927 (**A**) *t*-distributed stochastic neighbor embedding (*t*-SNE) projection plots showing epithelial cell
928 subpopulations in gingival tissue on Days 1, 4, and 7 following ligature placement. Colors indicate
929 cell type, as follows: dark green, epithelial cell population 1 (Epi 1); sea green, epithelial cell
930 population 2 (Epi 2); pale green, epithelial cell population 3 (Epi 3); light green, epithelial cell
931 population 4 (Epi 4); and light blue, epithelial cell population expressing epithelial–mesenchymal
932 transition (EMT) genes. (**B**) Heatmap showing expression of the top-10 differentially expressed
933 genes in Epi 1, Epi 2, Epi 3, Epi4, and EMT. (**C**) Violin plots showing gene expression levels of
934 keratin 5 (*Krt5*), keratin 14 (*Krt14*), cadherin 11 (*Cdh11*), *Col1a1*, tenascin C (*Tnc*), and smooth
935 muscle aortic actin 2 (*Acta2*) in epithelial cell subpopulations. (**D**) Violin plots showing gene
936 expression levels of interleukin 6 (*Il6*) and interleukin 23A (*Il23a*) in epithelial cell subpopulations.

Figure supplement 5

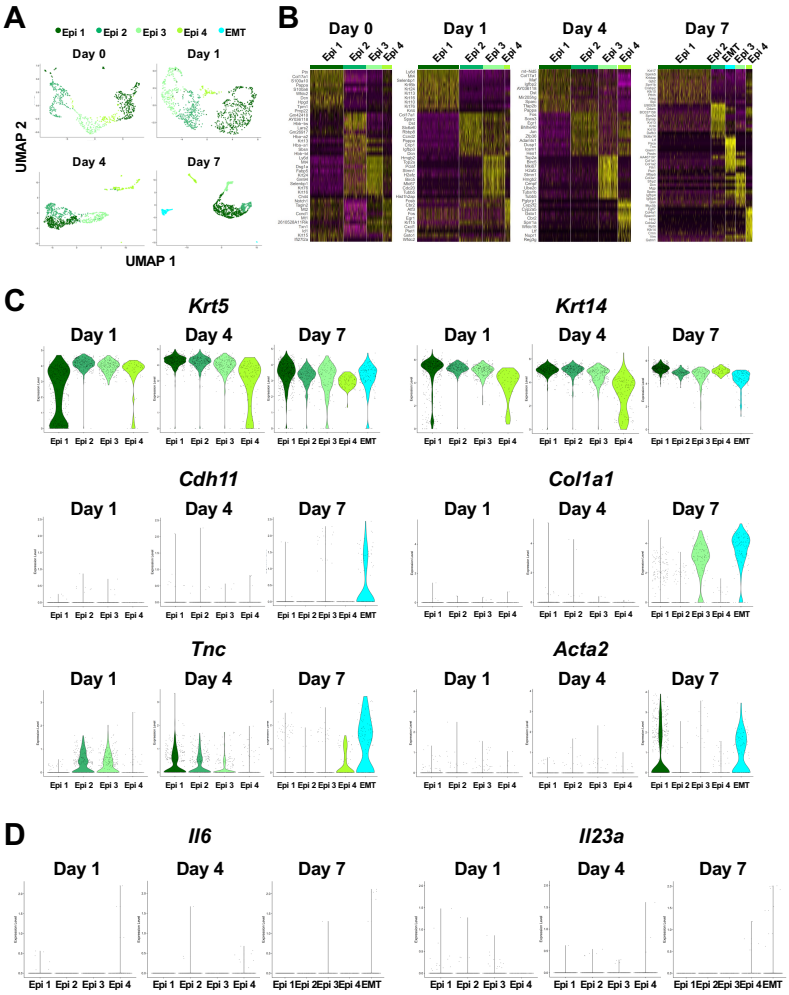

937